Effect of soil heterogeneity on seismic tunnel lining forces

G. Abate [*], S. Grasso, M.R. Massimino

Department of Civil Engineering and Architecture, University of Catania, Via Santa Sofia 64, 95124, Catania, Italy

A B S T R A C T

The crucial role that underground structures play today in transportation and utility networks makes their seismic vulnerability a fundamental topic.

The present paper deals with the role of soil heterogeneity in tunnel seismic behaviour. Starting from a real case history regarding a cross-section of the Catania (Italy) underground network, a finite element parametric study was carried out, focusing the attention on the soil discontinuity in terms of the impedance $\rho \bullet V_S$ of each layer crossed by the tunnel, being ρ and V_S the soil layer density and shear wave velocity, respectively. Different tunnel depths and seismic inputs were assumed. The numerical dynamic lining internal forces were compared with the analytical solutions proposed by Wang (1993) and Penzien (2000) for homogeneous soil deposits; two new approaches were proposed to use them for heterogeneous soils, highlighting the limitations of the original solutions and the range of applicability of the proposed approaches.

1. Introduction

Nowadays, tunnels are crucial components of the transportation and utility networks in urban areas. The considerable social and economic consequences of them being damaged denote the importance of their seismic design and vulnerability assessment, especially in areas characterized by high seismic risk. Although underground structures are usually less vulnerable to earthquakes compared to aboveground structures [1–5], the associated risk may be relevant, since even a low level of damage may affect the serviceability of a wide network. Post-earthquake observations [6–14] have demonstrated that underground structures may suffer severe damage due to earthquakes, as occurred in the 1995 Kobe (Japan), 1999 Chi-Chi (Taiwan) and 2004 Niigata (Japan) earthquakes, with catastrophic consequences for the entire urban area. The seismic behaviour of underground structures and particularly of tunnels is very distinct from that of aboveground structures [8,15].

The static design of tunnels has reached a high level of accuracy [16–19]; instead, a similar level of thoroughness in their seismic design has not yet been developed, mainly because of the complex soil-tunnel interaction phenomena that occur during an earthquake. The few existing design codes and guidelines about the seismic design of tunnels [20–22] and the numerous parameters that affect the dynamic response of soil-tunnel systems (*STSs*), have led the geotechnical research community to give great attention to the study of the dynamic response of

*STS*s [23–25].

Several methods are available in the literature for evaluating the seismic tunnel lining forces [8,26,27]. The results of these methods may significantly differ, even with the same design assumptions, due to both inherent epistemic uncertainties and a knowledge shortfall regarding some crucial issues that considerably affect the seismic response [28]. Moreover, no analytical solution takes specifically into account the heterogeneity of the soil crossed by the tunnel. Nevertheless, soil heterogeneity causes a complex soil response [29], which can influence significantly tunnel behaviour [30–32]. So, it is extremely important to consider it for *STS*s.

The present paper investigates the effects on the seismic tunnel lining forces of soil heterogeneity, in terms of the impedance $\rho \bullet V_S$ of each layer crossed by the tunnel, being ρ and V_S the soil layer density and shear wave velocity, respectively. A numerical parametric study was carried out by the ADINA FEM code [33,34], assuming different soil profiles. Starting from a cross-section of the underground network in Catania (Italy) in an 80 m stratified soil, different levels of soil heterogeneity, i. e., different values of $\rho \bullet V_S$, were adopted for the two soil layers crossed by the tunnel, maintaining constant the different values of $\rho \bullet V_S$ for all the other soil layers. Moreover, three soil-tunnel interface conditions were considered: the no-slip condition, the full-slip condition, and a partial-slip condition. Three different tunnel depths were investigated. Three seismic inputs were applied at the bedrock of the systems.

2D FEM models were developed in the tunnel transverse direction, as ovaling or racking deformations have the most significant influence on

List of symbols and abbreviations

a	Acceleration
a_g	Ground Acceleration
A	area
All	Alluvial soil
Agm-Agml	Sandy silty clays
Bvlc(F)-L1669	Volcanoclastic breccia of 1669
c	Dashpot coefficient
c'	Cohesion
c_u	Undrained cohesion
C	Compressibility ratio
$[C]$	Damping matrix
C_c	Soil facto controlling the shape of the spectra by enlarging the plateau at higher periods with respect to rock conditions
C_U	Class of use of a building according to the Italian Technical Code
d	Tunnel diameter
$D_s, D_s(\gamma)$	Soil damping ratio at the current shear strain, operative soil damping ratio
$D_{s,0}$	Soil damping ratio of soil at small strains, initial soil damping ratio
D_l	Tunnel lining damping ratio
EPB	Earth pressure balance
E_s	Soil Young modulus
$E_{s,0}$	Soil Young modulus at small strains
E_u	Undrained soil Young modulus
E_l	Tunnel lining Young modulus
f	frequency
f_{max}	Maximum frequency of the system
F	Flexibility ratio
F_0	Seismic parameter for the evaluation of the response spectrum, according to the Italian Technical Code (NTC 2018)
FEM	Finite Element Method
$G_s, G_s(\gamma)$	Soil shear modulus at the current shear strain, operative soil shear modulus
G_{s0}	Soil shear modulus at small strains, initial soil shear modulus
h	Mesh element size
H	Soil deposit height
HVSR	Horizontal-to-Vertical Spectral Ratio
I	Impedance ratio
I_l	Tunnel lining moment of inertia
k	Permeability
$[K]$	Stiffness matrix
Ls	Sandy silts
Lqua-L1669	Quartalaro Lava
$[M]$	Mass matrix
M	Dynamic bending moment
M_{ANAL}	Analytical dynamic bending moment
M_{MAX}	Maximum dynamic bending moment
M_{NUM}	Numerical dynamic bending moment
M_w	Moment magnitude
N	Dynamic axial force

N_{ANAL}	Analytical dynamic axial force
N_{MAX}	Maximum dynamic axial force
N_{NUM}	Numerical dynamic axial force
OP	Open-face
PHA	Peak horizontal acceleration
P_{VR}	Probability of exceeding for the evaluation of the seismic action, according to the Italian Technical Code
r	Radius of the tunnel lining
R_p	Anthropic layer
s	thickness of the tunnel lining
Sbv-L1669	Volcanic sand of 1669
SLO	Operating Limit State according to the Italian Technical Code (NTC 2018)
SLD	Damage Limit State according to the Italian Technical Code (NTC 2018)
SLV	Life-safety Limit State according to the Italian Technical Code (NTC 2018)
SLC	Collapse Prevention Limit State according to the Italian Technical Code (NTC 2018)
STS	Soil-Tunnel System
STSs	Soil-Tunnel Systems
t	time
TBM	Tunnel boring machine
T_R	Return period
T^*_c	Seismic parameter for the evaluation of the response spectrum, according to the Italian Technical Code (NTC 2018)
V_N	Nominal duration of a building
V_s	Soil shear waves velocity at the current shear strain, operative soil shear waves velocity
$V_{s, z=0}$	Soil shear waves velocity at the soil surface (z = 0)
$V_{s,av}$	Average Shear waves velocity
y	Horizontal direction
z	Vertical depth
α_r	First Rayleigh damping factor
β_r	Second Rayleigh damping factor
γ_s	Soil unit weight
γ	shear strain
γ_{max}	Soil maximum shear strain
ΔM	Percentage difference between $M_{NUM-MAX}$ and the $M_{ANAL-MAX}$
ΔN	Percentage difference between $N_{NUM-MAX}$ and the $N_{ANAL-MAX}$
Δz	Thickness of the soil cover above the tunnel, named "tunnel cover"
θ	centre angle of the tunnel
θ_r	centre angle of the tunnel crossing the soil discontinuity on the right of the tunnel
θ_l	centre angle of the tunnel crossing the soil discontinuity on the left of the tunnel
μ	friction coefficient
ν_s	Soil Poisson's ratio
ν_l	Tunnel Lining Poisson's ratio
ρ	soil density
φ	Shear strength angle
ω	Angular frequency

the tunnel lining forces under seismic loading [28,35]. A linear visco-elastic constitutive model was assumed for the tunnel. To consider soil nonlinearity, a linear-equivalent visco-elastic approach was assumed for the soil: operative values of the soil shear modulus G_s and damping ratio D_s according to the effective strain-stress level, i.e., in turn with the seismic input amplitude, were considered.

The response of the *STS* under examination was discussed in terms of dynamic lining internal forces, highlighting the extremely important role played by soil heterogeneity.

Finally, the analytical solutions proposed by Refs. [26,27] for homogeneous soil deposits were considered and modified to include soil heterogeneity. The results obtained using the modified analytical

solutions were compared with the FEM results. The comparison between the analytical and numerical results allows us to assess the validity and limitations of the modified analytical solutions.

2. The case-study

A cross-section of the underground network in Catania (Italy) was analysed. Section 2.1 reports the main information about the soil and the tunnel; Section 2.2 describes the seismic inputs applied at the base of the investigated *STS*.

2.1. Soil profile and tunnel characteristics

Fig. 1 a shows the whole network design: the red line indicates the two lines built in 1999 and currently in operation; the light blue lines indicate the two new lines at present under construction (Nesima-Misterbianco and Stesicoro-Palestro); the dark blue lines indicate the planned lines, which are not yet under construction. The cross-section analysed forms part of the light blue line between the stations of Nesima and Misterbianco [36–38]; it is next to the Si3 borehole (Figs. 1 and 2). The underground segment covers a length of 1748 m. Due to the strong soil heterogeneity in this area, the tunnel was dug using a Dual Mode Tunnel Boring Machine (TBM), switching frequently from the Open Face (OF) mode for the lava rock formations and the Earth Pressure Balance (EPB) mode for cohesive and/or incoherent soils. Geological and geotechnical information about the rocks and soils at the digging front was fundamental to define the appropriate digging mode and to choose the correct front pressure to guarantee the safety of the TBM and of the aboveground structures [39–49]. Geotechnical characterization was also fundamental to adequately estimate the soil profile and thus in turn the tunnel lining forces, as will be discussed in the next section.

The average digging depth was equal to about 25 m. The final tunnel lining consisted of a precast reinforced concrete ring; each ring consisted of 7 segments installed by an appropriate erector inside the TBM. The outside ring diameter was equal to 10 m. For the cross-section analysed, the tunnel cover was equal to 17 m (the axis is 22 m below the ground surface).

Many geotechnical characterizations of the soil have been performed in Catania over the years, due to its high seismic risk [50–56]. In particular, two different geotechnical investigations were performed to define the soil profile and the geotechnical parameters of the soils and rocks in the design phase of the Nesima-Misterbianco segment (Fig. 2 and Table 1): the first in 2004 during the preliminary design phase (see the 3 boreholes S2, S3 and S4 indicated in green in Fig. 2); the second in 2015 for the executive design phase (see the 15 boreholes Si1, Si2, Si3, Si4, Si4bis, Si5, Si6, Si7, Si8, Si9, Si9bis, Si10, Si11, Si12, Si13, indicated in red in Fig. 2). Furthermore, the investigations carried out in 1996 for the construction of a parking area around the Monte Pò station (see the 5 boreholes S1, S2, S3, S4, S5 indicated in black in Fig. 2) and those performed in 2000 as part of the "The Catania Project" ([57]; see the 3 boreholes S140, S1068, S1242 indicated in violet in Fig. 2) were also considered. Dilatometric Tests, Standard Penetration Tests, Permeability Lefranc Tests, absorption Lugeon Tests, Dac-Tests, Pocket Penetrometer Tests, Open Piezometer Tests, Down-Hole Tests and traditional Horizontal-to-Vertical Spectral Ratio (HVSR) Tests were performed. Table 2 reports the location of the main in-situ tests and the boreholes interested by the HVSR tests for the Nesima-Misterbianco segment. Many samples were also collected for laboratory tests.

Generally, an anthropic layer was found approaching the soil surface; then, lava rock layers were observed at greater depths. The geological formations involved in the digging process were essentially: volcanoclastic breccia and sand dating from 1669 from Si1 to Si8; Quartalaro lava from Si8 to Si10; volcanoclastic breccia dating from 1669 from Si10 to shortly beyond Si11; finally, Quartalaro lava up to Si13.

Fig. 1. (a) The underground network in Catania. (b) The Nesima-Misterbianco segment analysed, between the Nesima and Misterbianco stations.
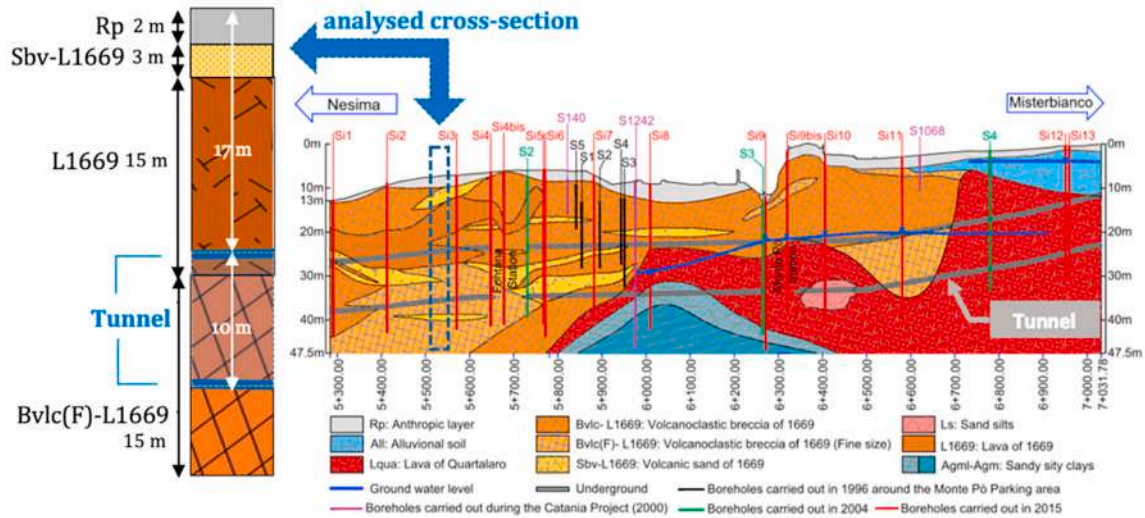
Fig. 2. Soil profile along the Nesima-Misterbianco segment and zoom on the analysed cross-section next to borehole Si3.

Table 1
Geotechnical parameters per each geological formation reported in Fig. 2.

Geological Formation	γ_s (kN/m^3)	φ' (°)	c' (kPa)	c_u (kPa)	V_S (m/s)	$E_{s,0}$ (MPa)	E_u (MPa)	k (m/s)
R_p	18 ÷ 19	30 ÷ 35	0 ÷ 10		120 ÷ 180	70 ÷ 125		
All	18 ÷ 21	20 ÷ 23	0 ÷ 10	70 ÷ 150	200 ÷ 350		20 ÷ 45	
Sbv-L1669	18 ÷ 21	32 ÷ 40	0 ÷ 20		200 ÷ 350	200 ÷ 400		10^{-5}
Agm	20 ÷ 21	18 ÷ 27	5 ÷ 30	100 ÷ 300	400 ÷ 550	1000		
Agml	20	18 ÷ 27	0 ÷ 15	200 ÷ 400	400 ÷ 550		55 ÷ 75	
Ls	19 ÷ 20	30 ÷ 35	0 ÷ 30	200 ÷ 400				10^{-5}
Bvlc-Bvlc(F)-L1669 (shallow layers)	18 ÷ 21	38 ÷ 45	0 ÷ 20		200 ÷ 350	250 ÷ 750		$10^{-6} ÷ 10^{-5}$
Lqua and L1669	25 ÷ 27	50 ÷ 65	100 ÷ 1000		550 ÷ 800	2000 ÷ 5000		$10^{-5} ÷ 10^{-3}$

Table 2
Mail in-situ tests performed along the Nesima-Misterbianco segment.

Geotechnical Survey	Borehole	Depth (m)	SPT	DMT	DH	HVSR
Executive Design Phase 2015 (see red labels in Fig. 2)	Si1	31	x	x	x	x
	Si2	34	x	x	x	x
	Si3	35	x			x
	Si4	35	x			x
	Si4bis	35	x			x
	Si5	35	x			x
	Si6	38	x			x
	Si7	33	x			x
	Si8	33	x			x
	Si9	35	x			x
	Si9bis	36	x			x
	Si10	38	x			x
	Si11	36	x			
	Si12	30				
	Si13	30				
Preliminary Design Phase 2004 (see green labels in Fig. 2)	S2	31	x		x	
	S3	30			x	
	S4	30				
Catania Project, 2000 (see violet labels in Fig. 2)	S140	8				
	S1068	10				
	S1242	45				
Construction of a parking area around the Monte Po Station (see black labels in Fig. 2)	S1	15	x		x	
	S2	15	x		x	
	S3	20	x			
	S4	15	x			
	S5	10				

As regards the cross-section under analysis (Fig. 2), the geological formations are: anthropic layer (Rp) for 0 m < z < 2 m, Volcanic sand of 1699 (Sbv-L1699) for 2 m < z < 5 m, Lava of 1669 (L1669) for 5 m < z <

20 m, and Volcanoclastic breccia of 1669 (Bvlc(F) – L1669) for 20 m < z < 35 m. The very thin layer of Bvlc-L1669 between L1669 and Bvlc(F)-L1669 and the very thin layer of Sbv-L1669 inside the Bvlc(F)-L1669 were not considered due to their very small thickness.

To define the geotechnical parameters of the investigated cross-section, data acquired from in-situ and laboratory tests were considered (Fig. 3).

Unfortunately, the investigation survey concerned a depth of about 30 m. The shear waves velocity measured at this depth was equal to 345 m/s (see black line in Fig. 3a), which is very far from 800 m/s, the minimum value of V_s for bedrocks according to the Italian and European technical regulations [58,59]. So, the V_s profile reported in Fig. 3 a as a red line was supposed (neglecting the rock layer at z = 5–20 m) to find the depth at which V_s = 800 m/s (conventional bedrock), according to the following expression:

$$V_s(z) = V_{s,z=0} + mz \tag{1}$$

being V_s = 235 m/s for z = 5 m and V_s = 345 m/s for z = 20 m according to the HVSR test next to borehole Si3 (see the black line in Fig. 3). This linear increase of the shear wave velocity with depth was considered representative for the site under analysis, based on the extensive geotechnical investigations that have involved the subsoil of the city of Catania over the years [37,48–53,56,57]]; [60–65].

Then, the value of the shear wave velocity at the soil surface, i.e. for z = 0, is $V_{s,z=0}$ = 198 m/s and the gradient of the red line is m = 22/3. According to equation (1), the bedrock was found at z = 80 m. So, the profile implemented in the FEM model discussed in Section 3 was reported in Fig. 3 a as a green line.

Table 3 reports the main geotechnical parameters for the cross-section analysed. According to Ref. [58], the soil is site class B (being
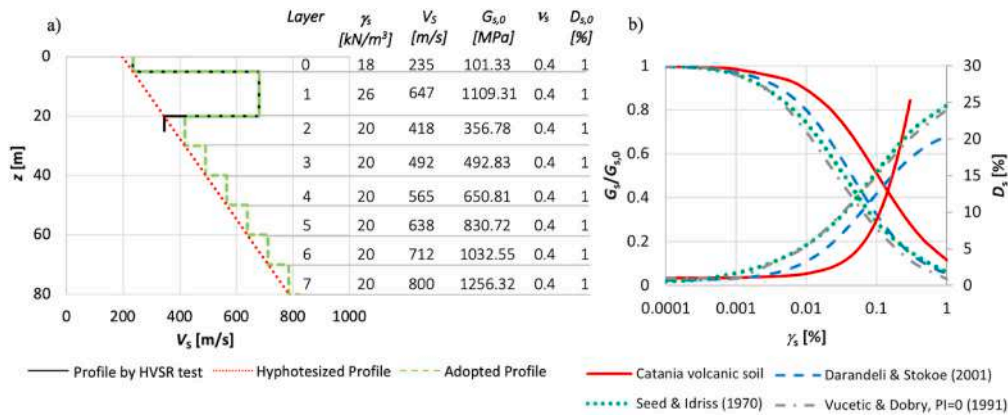
Fig. 3. a) $V_s(z)$ profile; b) $G_s/G_{s0}(\gamma)$ and $D_s(\gamma)$ curves used [53], compared to well-known literature curves [66–68].

Table 3
Geotechnical parameters for the analysed soil profile.

Soil Layer	Depth(m)	$\gamma_s(kN/m^3)$	$V_S(m/s)$	$\nu_s(-)$	$G_{s,0}(MPa)$	$E_{s,0}(MPa)$	$D_{s,0}(\%)$
0	0 ÷ 5	18	235	0.4	101.33	283.72	1
1	5 ÷ 20	26	647	0.4	1109.31	3106.07	1
2	20 ÷ 30	20	418	0.4	356.78	998.99	1
3	30 ÷ 40	20	492	0.4	492.83	1379.94	1
4	40 ÷ 50	20	565	0.4	650.81	1822.28	1
5	50 ÷ 60	20	638	0.4	830.72	2326.02	1
6	60 ÷ 70	20	712	0.4	1032.55	2891.16	1
7	70 ÷ 80	20	800	0.4	1256.32	3517.70	1

$V_{s,av} = 541$ m/s). Unfortunately, no specific dynamic laboratory tests were performed for the geological formations at the Si3 borehole. Thus, crudely the typical $G_s/G_{s0}(\gamma)$ and $D_s (\gamma)$ curves for Catania volcanic soil obtained by Ref. [53] were used (Fig. 3b) to consider the soil nonlinearity. For soil layer 1 in Fig. 3 a, which consists of compact Lava of 1669 (see L1669 layer in Fig. 2) $G_{s,0}$ and $D_{s,0}$ were used.

2.2. The seismic inputs adopted

Three different accelerograms were adopted for the analyses; they were scaled to *PHA = 0.383 g*, which is the expected value at the bedrock in the investigated area according to Ref. [58], considering the ultimate limit state associated with collapse or with other forms of structural failure which might endanger the safety of people (*SLV* in Table 4; $V_N =$ 100 years and $C_U = 2$).

Due to the lack of significant earthquake records for the city of Catania, just one recorded seismic input was used: that recorded during the 1990 earthquake at the Sortino station, resting on soil class A according to Ref. [58]. The other two seismic inputs were synthetic accelerograms according to the 1693 and 1818 scenario earthquakes for the city of Catania [69,70].

As shown in Fig. 4, the three seismic inputs differ as regards the frequency content. The 1990 seismic input has a predominant frequency

Table 4
Seismic parameters for the investigated area according to Ref. [58] (see the List of symbols and abbreviations reported at the end of the paper).

	T_R (years)	a_g (g)	M_w (*) (−)	F_0 (−)	T^*_c (s)	C_c (−)
SLO (P_{VR}=81%)	120	0.111 g	5.31	2.489	0.290	1.98
SLD (P_{VR}=63%)	201	0.140 g	5.46	2.461	0.313	1.92
SLV (P_{VR} = 10%)	**1898**	**0.383g**	**6.13**	**2.395**	**0.503**	**1.65**
SLC (P_{VR} = 5%)	2475	0.440 g	6.33	2.382	0.529	1.55

equal to 2 Hz. The Fourier spectrum of the 1693 seismic input is characterized by an amplitude mainly concentrated in two ranges of frequencies: 0.5–1 Hz and 4–5 Hz. The 1818 seismic input has a predominant frequency equal to 0.6 Hz.

The 1693 seismic input was used for the analyses whose results are discussed in Sections 5.1 and 5.2. The seismic inputs of all the three years, 1693, 1818 and 1990, were used for the analyses whose results are discussed in Section 5.3.

3. FEM modelling

To investigate the effects of soil heterogeneity, seismic inputs, and tunnel depths, the authors use the finite element method through the ADINA code [33,34,36–38,71–75]. Section 3.1. describes the FEM model developed for analysing the real cross-section. Section 3.2. describes the FEM models developed for analysing the effects of varying the soil discontinuity, in terms of the impedance $\rho \bullet V_S$ of each layer crossed by the tunnel, and the effects of the tunnel depth in relation to the previously mentioned soil discontinuity.

3.1. The real cross-section

To evaluate the seismic response of the *STS* described in Section 2, a 2D FEM model was performed. Fig. 5 a shows the mesh adopted; Fig. 5 b shows a zoom of the two soil layers crossed by the tunnel.

The 2D FEM model is 80 m deep (up to the hypothesized conventional bedrock) and 300 m wide ($\approx$4 times the soil depth), to reduce boundary effects [23,24]. The tunnel cover is $\Delta z = 17$ m from the soil surface and the tunnel is at a distance equal to 145 m from every vertical boundary. The soil was modelled by 4-node elements in plane strain conditions, and it was divided into 8 horizontal layers, according to the soil profile adopted (green line in Fig. 3a). The tunnel was modelled by 2-node beam elements. The mesh element size was chosen to ensure the following criteria: i) efficient reproduction of all the waveforms for the whole frequency range under study: $h \leq V_{s,min}/(6 \div 8 f_{max})$ [76]; ii) efficient modelling simulation of the soil next to the tunnel (therefore, a
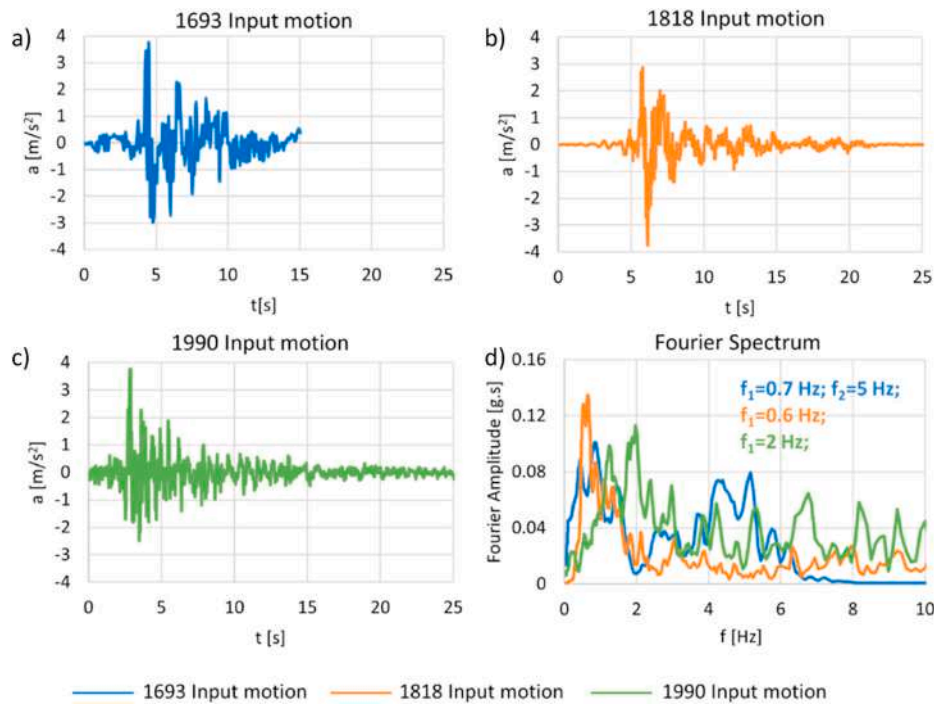
Fig. 4. a), b) and c) Adopted input motions scaled to PHA = 0.383 g according to Table 4; d) Their Fourier spectra.
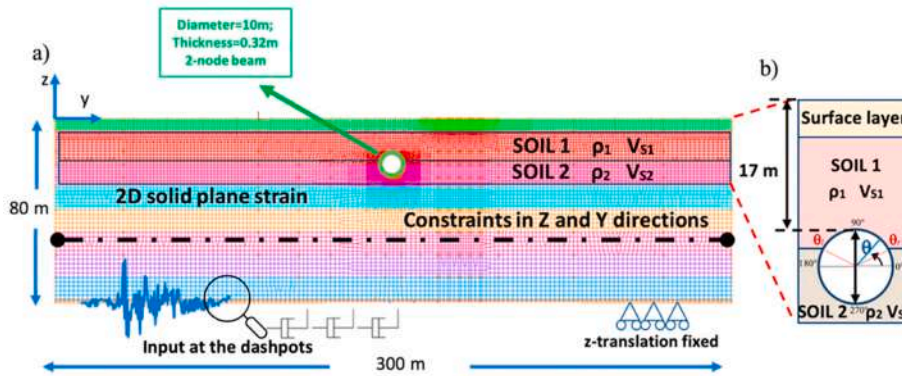

Fig. 5. (a) FEM model; (b) Zoom of the two soil layers crossed by the tunnel.

finer discretization near the tunnel was selected).

As regards the boundary conditions, the nodes of the soil vertical boundaries were linked by *"constraint equations"* that imposed the same horizontal and vertical displacements at the same depths to reproduce the typical free-field conditions in site response analyses [74,77–79]. The base of the model was constrained only in the vertical direction. Moreover, dashpots were implemented at the base of the model, to simulate the elastic bedrock according to Ref. [80]. The dashpot coefficient was defined as $c = \rho \cdot V_S \cdot A$, being: ρ the mass density of the bedrock; V_S the shear wave velocity of the bedrock and A the dashpot influence area. The earthquake excitations were applied as acceleration time histories (see Section 2.2) to these dashpots, as required by the ADINA FEM code utilised, and other FEM codes [33,34,71–75].

Modelling the tunnel-soil interface represents a key-aspect for detecting the dynamic response of tunnels [81–84]. To model the interface, the ADINA code used requires the definition of a "contact group" made by two "contact lines" ("contact surfaces" in 3D analyses), the most rigid is defined as the "target line" and the most flexible is defined as the "contactor line". Then, the code requires the definition of a "contact pair" to match the "contactor" and "target" lines, and it must

be characterized by the definition of the "Coulomb friction coefficient" (μ) between the "target line" and the "contactor line". If $\mu = 1$ the "target line" and the "contactor line" cannot slide relative to each other (no-slip condition); if $\mu = 0$ the "contactor line" is completely free to slide on the "target line" and vice versa (full-slip condition); if $0 < \mu < 1$ the relative sliding between the two surfaces can occur when the sliding action is greater than the friction resistance (partial-slip condition).

In the investigated FEM models, considering that the racking deformation of the tunnel under examination is amplified compared with the soil deformation (the flexibility ratio F was significantly higher than 1 – see Section 4), the soil line around the tunnel was defined as "target line" and the tunnel as "contactor line".

As regards the "Coulomb friction coefficient", initially (see Section 5.1, Models 1–4), the authors analysed three different interface conditions: the no-slip condition, the full-slip one and a partial-slip one, according to the tunnel-soil interface conditions considered by Refs. [26, 27]. So, the Authors assumed the following three different values: $\mu = 1$, $\mu = 0$, $\mu = 0.5$, respectively. The investigation of Models 1–4 showed that very similar results were obtained in terms of tunnel bending moments considering all the three interface conditions; higher values of the tunnel

axial forces were reached in the no-slip condition (see Section 5.1). Thus, the authors used only the no-slip condition for all the other FEM models developed, as shown in Section 5.2 for Models 1–10 and in Section 5.3 for Models 3-a and 3.b.

A linear-equivalent-visco-elastic approach was used for the soil. To consider soil nonlinearity, operative V_s, G_s and D_s values were retrieved from the FEM simulations at the end of the running according to the $G_s/G_{s0}(\gamma)$ and $D_s(\gamma)$ curves shown in Fig. 3 b and so in turn according to the achieved shear strains for each soil layer, thanks to a developed iterative procedure. These achieved shear strains in the soil obviously depend on the applied inputs and so in turn the operative V_s, G_s and D_s values vary with the applied inputs. For "Soil 1", i.e., the soil layer between 5 m and 20 m, $G_{s,0}$ and $D_{s,0}$ were adopted because it is a very stiff layer. Table 5 shows both the initial values and the operative values of shear modulus and damping ratio, as well as the shear modulus reduction and the damping ratio increase for each layer and for the three different seismic inputs.

A linear visco-elastic constitutive model was used for the tunnel, using the following values: $E_l = 36,283$ MPa, $\nu_l = 0.2$ and $D_l = 5\%$.

Finally, the damping matrix $[C]$ is defined as a combination of the mass matrix $[M]$ and the stiffness matrix $[K]$, according to the Rayleigh damping approach [85]:

$$[C] = \alpha_r[M] + \beta_r[K] \tag{2}$$

For the calibration of the Rayleigh coefficients α_r and β_r, the double frequency approach was used [86]:

$$\alpha_r = 2 \bullet \frac{D \bullet \omega_i \bullet \omega_j}{\omega_i + \omega_j}; \; \beta_r = 2 \bullet \frac{D}{\omega_i + \omega_j} \tag{3}$$

As for the soil, $\omega_i = \omega_1 = \frac{V_{S,av}}{4H} 2\pi$ and $\omega_j = n \bullet \omega_1$. According to Ref. [86], for soil with a thickness greater than 50 m, it is advisable to consider the contributions of the higher modes. The value of "n" was chosen to obtain the damping within an essentially constant period range: it is usually in the range $3 \div 6$. The authors assumed $n = 3$. Fig. 6

shows the Rayleigh coefficients obtained for the three seismic inputs. The frequencies ω_i and ω_j for the tunnel were assumed equal to those calculated for the soil, because the tunnel and the soil, being closely related, respond approximately in agreement to the movement induced by the earthquake. Alternative calibration of Rayleigh damping can be found in Ref. [87].

3.2. The parametric analyses

Usually, dynamic analyses of coupled *STSs* are performed considering a homogeneous soil at the tunnel level [88]. However, soil heterogeneity in terms of soil density and shear wave velocity can significantly influence the soil-tunnel dynamic behaviour. Thus, starting from the real case history, the present work deals with numerous parametric analyses carried out considering at the tunnel level different values of the impedance ratio I, defined as:

$$I = (\rho_1 \bullet V_{S1}) / (\rho_2 \bullet V_{S2}) \tag{4}$$

where $\rho_1 \bullet V_{S1}$ is the impedance of the soil interacting with the upper part of the tunnel ("Soil 1") and $\rho_2 \bullet V_{S2}$ is the impedance of the soil interacting with the bottom part of the tunnel ("Soil 2"), being ρ_1 and V_{S1} the density and the operative shear wave velocity of "Soil 1", and ρ_2 and V_{S2} the density and the operative shear wave velocity of "Soil 2", respectively (Fig. 5).

So, the geotechnical parameters of "Soil 1" and "Soil 2" were modified to obtain ten different values of I, developing ten different models (Table 6).

Initially, Models 1–4 (Table 6) were investigated. Model 3 ($I = 2.6$) refers to the real soil profile; Model 1 ($I = 1.0$) refers to a homogeneous soil crossed by the tunnel. As previously stated, for Models 1–4 three different tunnel-soil interface conditions (full-slip, no-slip, partial-slip) were used.

Then, Models 5–10 (Table 6) were investigated. As stated above, only the no-slip tunnel-soil interface condition was modelled for these

Table 5
Soil dynamic parameters for the three adopted seismic inputs.

		Initial values				Operative values[a]				
		1693 seismic event								
Depth, z (m)	ρ_s (kNs2/m4)	ν_s (−)	G s,0 (MPa)	D s,0 (%)		Gs (MPa)	Gs/Gs0 (−)	Vs (m/s)	Ds (%)	Ds/Ds,0 (−)
0 ÷ 5	1.83	0.4	101.33	1		79.69	0.78	209	4	4
5 ÷ 20	2.65	0.4	1109.31	1		1109.31	1.00	647	1	1
20 ÷ 30	2.04	0.4	356.78	1		212.43	0.60	323	4	4
30 ÷ 40	2.04	0.4	492.83	1		327.68	0.66	401	4	4
40 ÷ 50	2.04	0.4	650.81	1		468.19	0.72	479	4	4
50 ÷ 60	2.04	0.4	830.72	1		604.63	0.73	544	4	4
60 ÷ 70	2.04	0.4	1032.55	1		767.33	0.74	613	4	4
70 ÷ 80	2.04	0.4	1256.32	1		958.26	0.76	685	4	4
		1818 seismic event								
Depth, z (m)	ρ_s (kNs2/m4)	ν_s (−)	G s,0 (MPa)	D s,0 (%)		Gs (MPa)	Gs/Gs0 (−)	Vs (m/s)	Ds (%)	Ds/Ds,0 (−)
0 ÷ 5	1.83	0.4	101.33	1		71.14	0.70	197	5	5
5 ÷ 20	2.65	0.4	1109.31	1		1109.31	1.00	647	1	1
20 ÷ 30	2.04	0.4	356.78	1		183.42	0.51	300	5	5
30 ÷ 40	2.04	0.4	492.83	1		277.56	0.56	369	5	5
40 ÷ 50	2.04	0.4	650.81	1		399.45	0.61	443	5	5
50 ÷ 60	2.04	0.4	830.72	1		540.76	0.65	515	5	5
60 ÷ 70	2.04	0.4	1032.55	1		708.89	0.69	590	5	5
70 ÷ 80	2.04	0.4	1256.32	1		906.69	0.72	667	5	5
		1990 seismic event								
Depth, z (m)	ρ_s (kNs2/m4)	ν_s (−)	G s,0 (MPa)	D s,0 (%)		Gs (MPa)	Gs/Gs0 (−)	Vs (m/s)	Ds (%)	Ds/Ds,0 (−)
0 ÷ 5	1.83	0.4	101.33	1		80.61	0.80	210	3	3
5 ÷ 20	2.65	0.4	1109.31	1		1109.31	1.00	647	1	1
20 ÷ 30	2.04	0.4	356.78	1		213.96	0.60	324	3	3
30 ÷ 40	2.04	0.4	492.83	1		328.83	0.67	402	3	3
40 ÷ 50	2.04	0.4	650.81	1		479.15	0.74	485	3	3
50 ÷ 60	2.04	0.4	830.72	1		637.47	0.77	559	3	3
60 ÷ 70	2.04	0.4	1032.55	1		815.09	0.79	632	3	3
70 ÷ 80	2.04	0.4	1256.32	1		1018.79	0.81	707	3	3

[a] Final dynamic properties adopted to consider soil nonlinearity in the FEM modelling, evaluated considering the effective shear strains due to every applied seismic input.
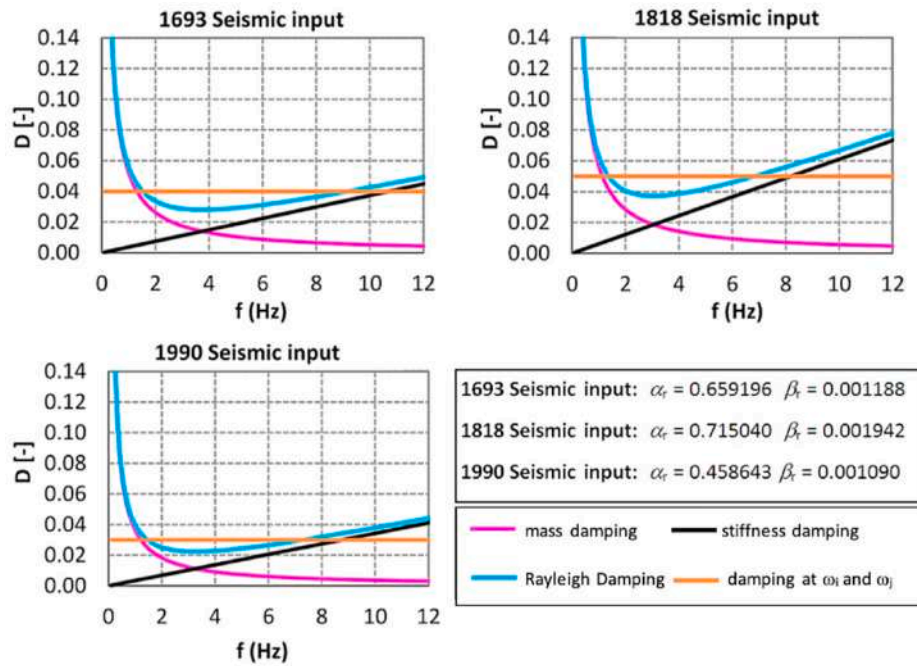
Fig. 6. Rayleigh damping curves and parameters used in the FEM modelling.

Table 6

Main equivalent soil parameters for the two soil layers crossed by the tunnel for Models 1–10.

		Model 1 I = 1.0			Model 2 I = 2.0		
Soil Layer	*Depth(m)*	$\rho_s(kNs^2/m^4)$	$V_S(m/s)$		$\rho_s(kNs^2/m^4)$	$V_S(m/s)$	
1	5 ÷ 20	2.04	323		2.65	496	
2	20 ÷ 30	2.04	323		2.04	323	
		Model 3 I = 2.6			*Model 4 I = 3.5*		
	Depth(m)	$\rho_s(kNs^2/m^4)$	$V_S(m/s)$		$\rho_s(kNs^2/m^4)$	$V_S(m/s)$	
1	5 ÷ 20	2.65	647		2.65	647	
2	20 ÷ 30	2.04	323		2.04	240	
		Model 5 I = 1.5			*Model 6 I = 1.5*		
	Depth(m)	$\rho_s(kNs^2/m^4)$	$V_S(m/s)$		$\rho_s(kNs^2/m^4)$	$V_S(m/s)$	
1	5 ÷ 20	2.65	647		2.65	647	
2	20 ÷ 30	2.04	560		2.65	431	
		Model 7 I = 3.0			*Model 8 I = 0.5*		
	Depth (m)	$\rho_s(kNs^2/m^4)$	$V_S(m/s)$		$\rho_s(kNs^2/m^4)$	$V_S(m/s)$	
1	5 ÷ 20	2.65	647		2.04	323	
2	20 ÷ 30	2.04	280		2.65	496	
		Model 9 I = 0.3			*Model 10 I = 4.0*		
	Depth(m)	$\rho_s(kNs^2/m^4)$	$V_S(m/s)$		$\rho_s(kNs^2/m^4)$	$V_S(m/s)$	
1	5 ÷ 20	2.04	240		2.65	647	
2	20 ÷ 30	2.65	647		2.04	210	

Table 7

Main characteristics of all the FEM models developed.

Model	Applied seismic input	Tunnel-soil interface condition	Δz (m)	I
1	1693	no-slip condition (μ = 1)	17	1.0
	1693	full-slip condition (μ = 0)	17	1.0
	1693	partial-slip condition (μ = 0.5)	17	1.0
2	1693	no-slip condition (μ = 1)	17	2.0
	1693	full-slip condition (μ = 0)	17	2.0
	1693	partial-slip condition (μ = 0.5)	17	2.0
3	1693	no-slip condition (μ = 1)	17	2.6
	1693	full-slip condition (μ = 0)	17	2.6
	1693	partial-slip condition (μ = 0.5)	17	2.6
3a	1693	no-slip condition (μ = 1)	12	2.6
	1818	no-slip condition (μ = 1)	12	2.6
	1990	no-slip condition (μ = 1)	12	2.6
3b	1693	no-slip condition (μ = 1)	7	2.6
	1818	no-slip condition (μ = 1)	7	2.6
	1990	no-slip condition (μ = 1)	7	2.6
4	1693	no-slip condition (μ = 1)	17	3.5
	1693	full-slip condition (μ = 0)	17	3.5
	1693	partial-slip condition (μ = 0.5)	17	3.5
5	1693	no-slip condition (μ = 1)	17	1.5
6	1693	no-slip condition (μ = 1)	17	1.5
7	1693	no-slip condition (μ = 1)	17	3.0
8	1693	no-slip condition (μ = 1)	17	0.5
9	1693	no-slip condition (μ = 1)	17	0.3
10	1693	no-slip condition (μ = 1)	17	4.0

additional models.

Finally, the tunnel depth was modified. Starting from Model 3 having a tunnel cover equal to $\Delta z = 17$ m, two other models were performed: in Model 3-a $\Delta z = 12$ m and in Model 3-b $\Delta z = 7$ m were assumed. For the original tunnel cover $\Delta z = 17$ m, the tunnel crossed 3 m of "Soil 1" and 7 m of "Soil 2"; for $\Delta z = 12$ m, the tunnel crossed 8 m of "Soil 1" and 2 m of "Soil 2"; for $\Delta z = 7$ m, the tunnel crossed only "Soil 1" (Figs. 2 and 5).

For all the analyses focused on the effects of *I*, the 1693 seismic input was used. For the analyses focused on the effects of the tunnel depth the 1818 and 1990 seismic inputs were also used, thus considering the effect of different inputs on the tunnel behaviour as well.

Table 7 reports the seismic inputs, tunnel-soil interface conditions, the tunnel cover, Δz, and the impedance ratio, *I*, used for all the investigated FEM models.

4. Analytical solutions used to evaluate the dynamic lining internal forces

The response of the *STS* was discussed in terms of lining internal forces. These quantities were evaluated not only through the FEM analyses but also using the closed-form solutions proposed by Refs. [26,27], modified as will be discussed later in the section. Wang [26] and Penzien [27] solutions are commonly used in the preliminary design stages of tunnels and based on these assumptions: a) the soil is an infinite, elastic, homogeneous, isotropic medium; b) the circular lining is generally an elastic medium under plane strain conditions.

The response of the tunnel lining is expressed as a function of the compressibility and flexibility ratios (*C* and *F*) of the tunnel, which are

respectively measures of the extensional and flexural stiffness of the soil relative to the tunnel; they are given by Ref. [89]:

$$C = \frac{E_s(1-\nu_l^2)r}{E_l s(1+\nu_s)(1-2\nu_s)} \tag{5}$$

$$F = \frac{E_s(1-\nu_l^2)r^3}{6E_l I_l(1+\nu_s)} \tag{6}$$

where E_s is the soil Young modulus, ν_s is the soil Poisson's ratio, E_l is the tunnel Young modulus, ν_l is the lining Poisson's ratio, I_l is the tunnel moment of inertia (per meter) and r and s are respectively the radius and the thickness of the tunnel. For $F \to 0$ the tunnel is rigid and will not show deformations. For $0 < F < 1$ the tunnel is stiffer than the soil, thus the tunnel deformation will be smaller than the soil deformation (rigid tunnel). For $F = 1$ the tunnel and the soil have the same level of stiffness, so the tunnel will follow the free-field deformation. For $F > 1$ the racking deformation of the tunnel is amplified compared with the soil deformation (flexible tunnel).

For Models 1–10 it was significantly $F > 1$.

Wang [26] proposed the expressions (7-11) for evaluating the maximum bending moment M_{MAX} and the maximum axial force N_{MAX}, in the lining per unit of longitudinal dimension, due to seismic loadings.

For both the full-slip and no-slip conditions at the soil-tunnel interface, M_{MAX} can be computed as:

$$M_{MAX} = \pm\frac{1}{6}K_1\frac{E_s}{(1+\nu_s)}r^2\gamma_{max} \tag{7}$$

where:

$$K_1 = \frac{12(1-\nu_s)}{2F+5-6\nu_s} \tag{8}$$

and γ_{max} is the soil maximum shear strain at the tunnel depth.

As regards N_{MAX}, for the full-slip condition it can be computed as:

$$N_{MAX} = \pm\frac{1}{6}K_1\frac{E_s}{(1+\nu_s)}r\gamma_{max} \tag{9}$$

For the no-slip condition N_{MAX} can be computed as:

$$N_{MAX} = \pm K_2\frac{E_s}{2(1+\nu_s)}r\gamma_{max} \tag{10}$$

where:

$$K_2 = 1 + \frac{F[(1-2\nu_s)-(1-2\nu_s)C]-\frac{1}{2}(1-2\nu_s)^2+2}{F[(3-2\nu_s)+(1-2\nu_s)C]+C\left(\frac{5}{2}-8\nu_s+6\nu_s^2\right)+6-8\nu_s} \tag{11}$$

Penzien [27] developed similar closed-form solutions, proposing the expressions (12–19) for evaluating the bending moment $M(\theta)$ and the axial force $N(\theta)$, being θ the centre angle of the tunnel (see Fig. 5b).

Assuming the full-slip condition, the bending moments and the axial forces can be computed as:

$$M(\theta) = \pm\frac{3E_l I_l R^n\gamma_{max}}{d(1-\nu_l^2)}\cos 2\left(\theta+\frac{\pi}{4}\right) \tag{12}$$

$$N(\theta) = \pm\frac{6E_l I_l R^n\gamma_{max}}{d^2(1-\nu_l^2)}\cos 2\left(\theta+\frac{\pi}{4}\right) \tag{13}$$

where:

$$R^n = \pm\frac{4(1-\nu_s)}{(\alpha^n+1)} \tag{14}$$

$$\alpha^n = \frac{12E_l I_l(5-6\nu_s)}{d^3G_s(1-\nu_l^2)} \tag{15}$$

Assuming the no-slip condition, the bending moments and the axial

forces can be computed as:

$$M(\theta) = \pm\frac{3E_l I_l R\gamma_{max}}{d(1-\nu_l^2)}\cos 2\left(\theta+\frac{\pi}{4}\right) \tag{16}$$

$$N(\theta) = \pm\frac{12E_l I_l R\gamma_{max}}{d^2(1-\nu_l^2)}\cos 2\left(\theta+\frac{\pi}{4}\right) \tag{17}$$

where:

$$R = \pm\frac{4(1-\nu_s)}{(\alpha+1)} \tag{18}$$

$$\alpha = \frac{24E_l I_l(3-4\nu_s)}{d^3G_s(1-\nu_l^2)} \tag{19}$$

As previously mentioned, expressions (7-19) were developed for tunnels in homogeneous soil. So, the authors fit them for the heterogeneous soil profile under analysis, adopting the following two different approaches.

- **Approach N. 1:** Considering the anticlockwise, for θ from θ_r to θ_l, crossing the tunnel "Soil 1", E_S (or G_S) of "Soil 1" was used; for θ from θ_l to θ_r, crossing the tunnel "Soil 2", E_S (or G_S) of "Soil 2" was used, being θ_r the centre angle of the tunnel crossing the soil discontinuity on the right of the tunnel vertical axis and θ_l the centre angle of the tunnel crossing the soil discontinuity on the left of the tunnel vertical axis (see Fig. 5b). These angles assume different values considering the different hypothesized tunnel covers: for $\Delta z = 17$ m, $\theta_r = 24°$ and $\theta_l = 156°$, while for $\Delta z = 12$ m it is $\theta_r = 323°$ and $\theta_l = 217°$; finally, for $\Delta z = 7$ m the tunnel crosses only "Soil 1". As for the soil maximum shear strain at the tunnel depth, for $0° < \theta < 360°$ a unique value of γ_{max} was considered as the average value of the maxima soil shear strains for 17 m $\leq$ z $\leq$ 27 m, i.e., along the tunnel.
- **Approach N. 2:** Considering the anticlockwise, for θ from θ_r to θ_l, crossing the tunnel "Soil 1", E_S (or G_S) of "Soil 1" was used; for θ from θ_l to θ_r, crossing the tunnel "Soil 2", E_S (or G_S) of "Soil 2" was used, as assumed in the previous Approach N. 1. Nevertheless, unlike the previous approach, two different values of γ_{max} were considered: the first one is the average value of the maxima soil shear strains for "Soil 1", i.e., for θ from θ_r to θ_l; the second one is the average value of the maxima soil shear strains for "Soil 2", i.e., for θ from θ_l to θ_r.

5. Results in terms of tunnel bending moment (*M*) and axial force (*N*)

The authors investigate the response of the *STSs* under examination in terms of dynamic lining internal forces. Section 5.1. shows the effect of the soil stiffness discontinuity and of the tunnel-soil interface conditions on the tunnel dynamic lining forces, *M* and *N*, for *I* in the range 1.0–3.5 (Models 1–4). Section 5.2. show the effect of the soil stiffness discontinuity on *M* and *N* for the tunnel-soil no-slip condition and *I* in the range 0.3–4.0 (Models 1–10). Finally, Section 5.3. shows the effects of the tunnel depth and of the seismic inputs on *M* and *N* for the tunnel-soil no-slip condition and *I* = 2.6 (Model 3). For the main characteristics of all the investigated models see also Table 7.

5.1. Effects of I and tunnel-soil interface conditions on M and N: results concerning models 1–4 (I = 1.0–3.5)

As previously stated, the results reported in this section were obtained considering the 1693 seismic input. All the tunnel-soil interface conditions discussed in Section 3 were considered. Figs. 7 and 8 show, respectively, the numerical seismic bending moments *M* and axial force *N* computed along the tunnel for Models 1–4. Two different coloured bands highlight the two different soil layers crossed by the tunnel: pink refers to "Soil 1" interacting with the upper part of the tunnel, beige
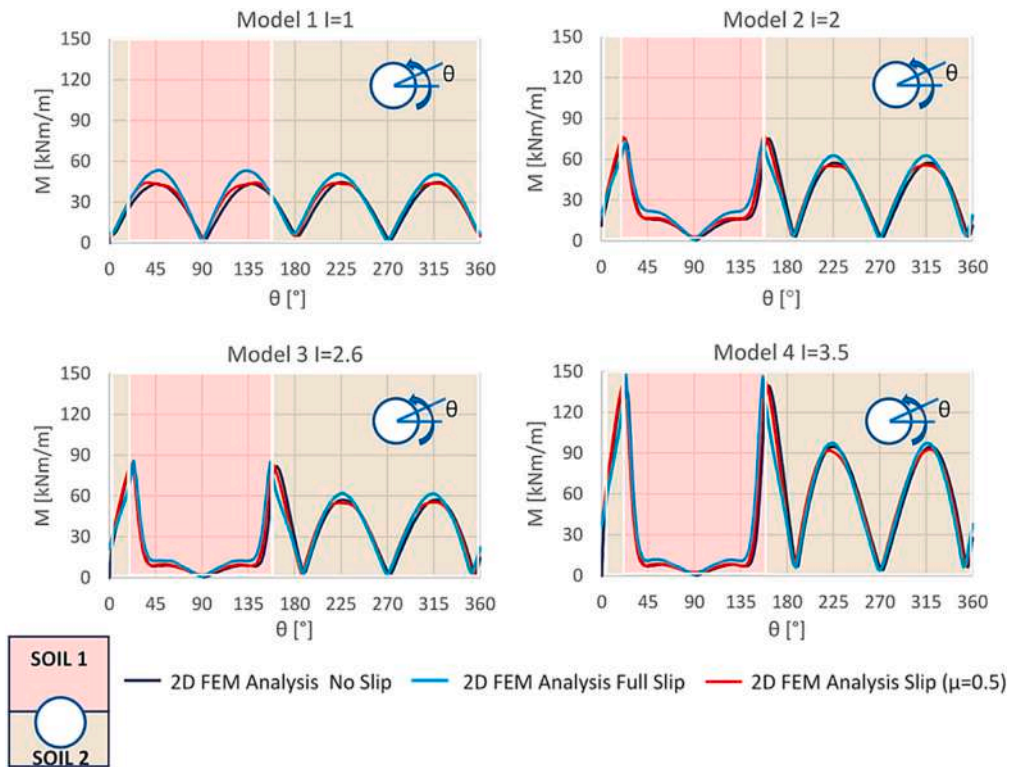
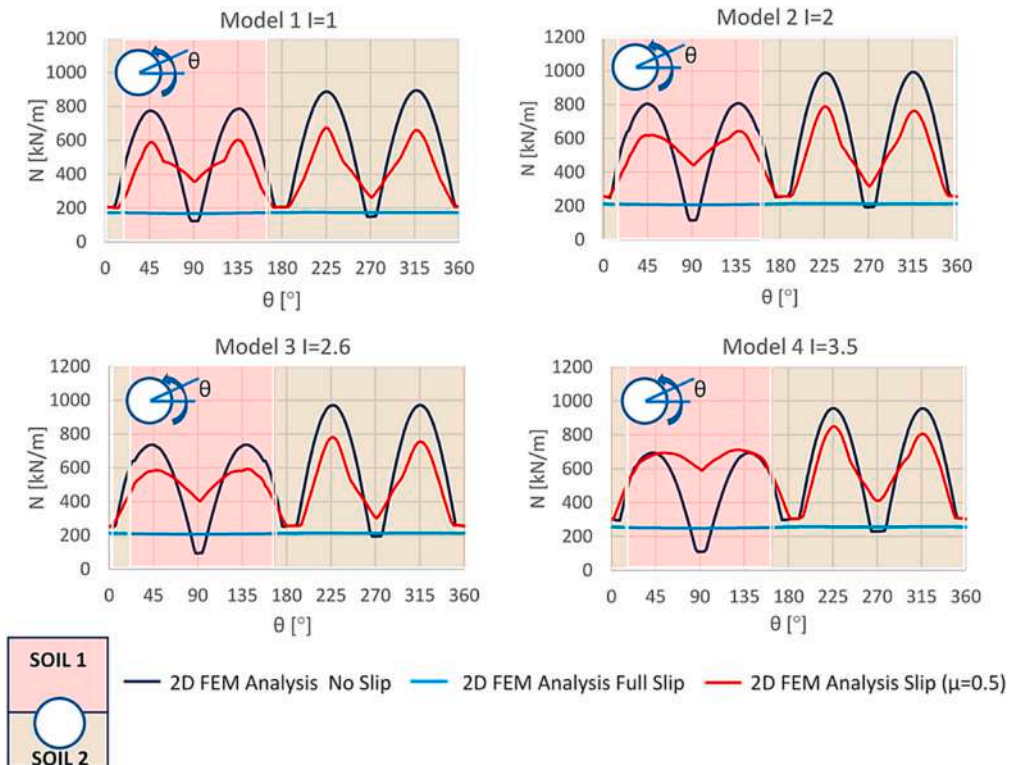Fig. 7. Numerical dynamic bending moments for Models 1–4.

Fig. 8. Numerical dynamic axial forces for Models 1–4.

refers to "Soil 2" interacting with the bottom part of the tunnel.

The strong influence exerted by the soil heterogeneity was found in the M distribution (Fig. 7). As expected, the best distribution of M was obtained for Model 1, representing the homogeneous soil condition at

the tunnel depth ($I = 1.0$). For higher values of I, higher values of M were evaluated, resulting in a strongly non-uniform bending moment distribution along the tunnel. Smaller bending moments were found at the depth of "Soil 1" (stiff soil); higher values were obtained at the depth of

"Soil 2" (soft soil), with important peaks at the soil stiffness discontinuity. The soil stiffness discontinuity produces the evident peaks of the bending moment exactly at the soil stiffness discontinuity. The greater the soil stiffness discontinuity, the greater the bending moment peak, i. e., the peaks increased as I increased. Passing from $I = 1$ to $I = 3.5$ M_{MAX} grew by about 200%.

Therefore, it is advisable to carefully evaluate bending moment distributions for a tunnel crossing heterogeneous soil and to perform the necessary geotechnical in-situ tests to precisely estimate the depth of the soil stiffness discontinuity and the impedance ratio I. As for the three different tunnel-soil interface conditions, very similar results were

achieved (Fig. 7).

Unlike the bending moments, the axial forces obtained did not vary much with I, because axial forces are not so influenced by the soil deformation trend around the tunnel (Fig. 8). Nevertheless, the values of the axial forces are lightly different in the two parts of the tunnel inside "Soil 1" and inside "Soil 2", respectively. Regarding the three different soil-tunnel interfaces, higher values of axial forces were reached in the no-slip condition, due to the higher concentration of stress along the tunnel, generated by a lack of relative sliding between the soil and the tunnel. For the partial-slip condition, around 20% lower values were obtained. Finally, for the full-slip condition, constant low values (about
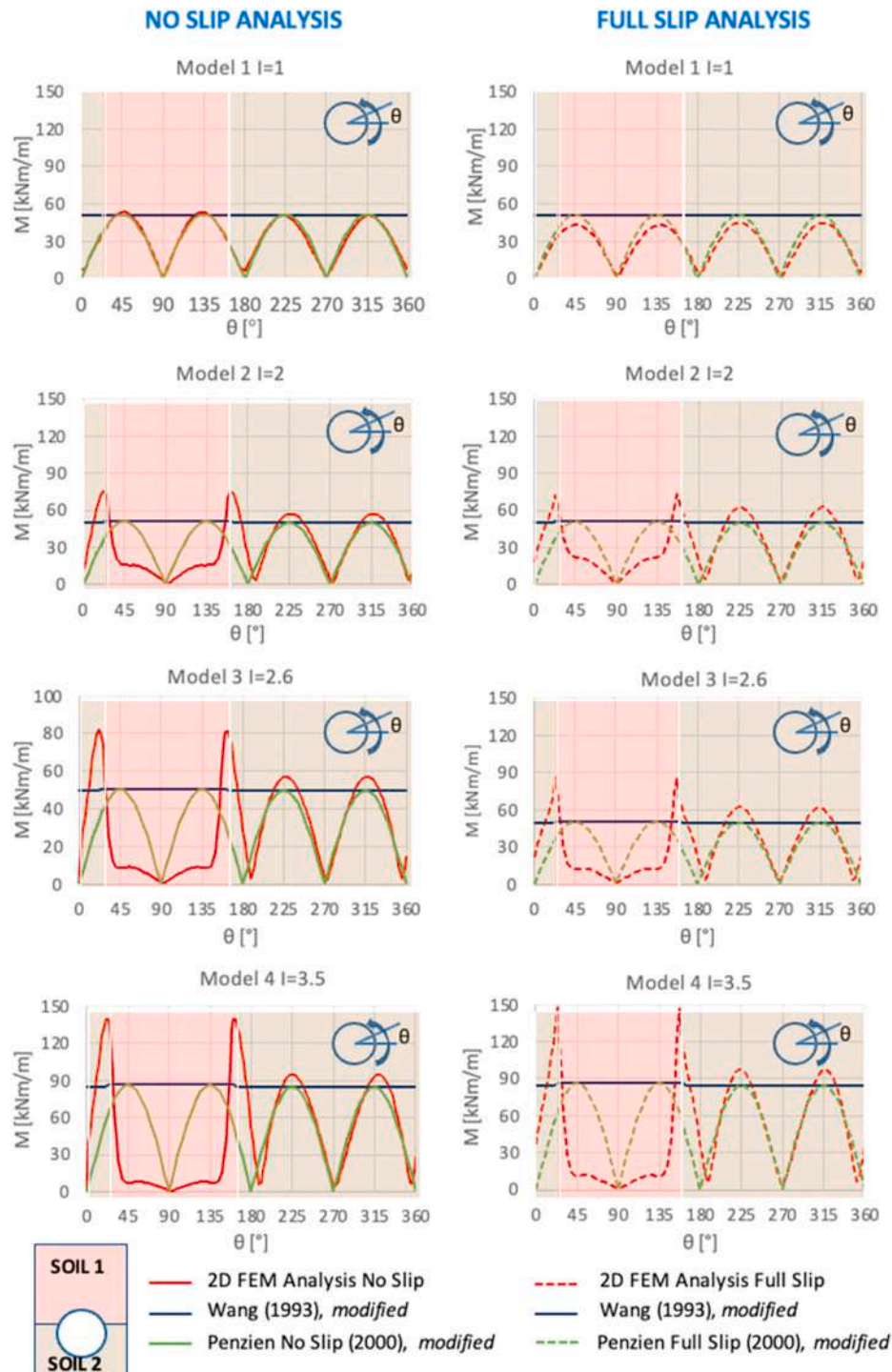
Fig. 9. Comparison between analytical (Approach N.1) and numerical results in terms of dynamic bending moments.

200 kN/m) were found.

The results shown in Figs. 7 and 8 were also compared with those obtained using the analytical solutions developed for both the no-slip and full-slip conditions by Refs. [26,27] modified according to Approach N.1, described in Section 4.

Fig. 9 shows the comparison for Models 1–4 in terms of bending moments. The numerical results achieved for Model 1 ($I = 1$) were very similar to the analytical solutions for both the interface conditions (no-slip and full-slip). For $I > 1.0$ a disagreement between analytical and numerical results was obtained. The highest degree of difference between $M_{NUM-MAX}$ and the $M_{ANAL-MAX}$ is equal to about 70% ($I = 3.5$, Model 4). The analytical solutions underestimated the bending

moments, and they were not able to reproduce the strong effect of the soil heterogeneity on the M distribution.

Similarly, Fig. 10 shows the comparisons between the analytical axial forces and the numerical ones. A great disagreement was often obtained. A good agreement is achieved only for Model 1 ($I = 1$, homogeneous soil) considering the Wang solution [26] for the no-slip interface condition. Very low values were achieved using the Penzien solutions [27], as found by other studies [88]. An increase in I leads to a greater disagreement between the analytical and numerical results, and the strongest disagreement was found for the full-slip interface condition. disagreement was found for the full-slip interface condition.

As previously explained, the analytical solutions require the
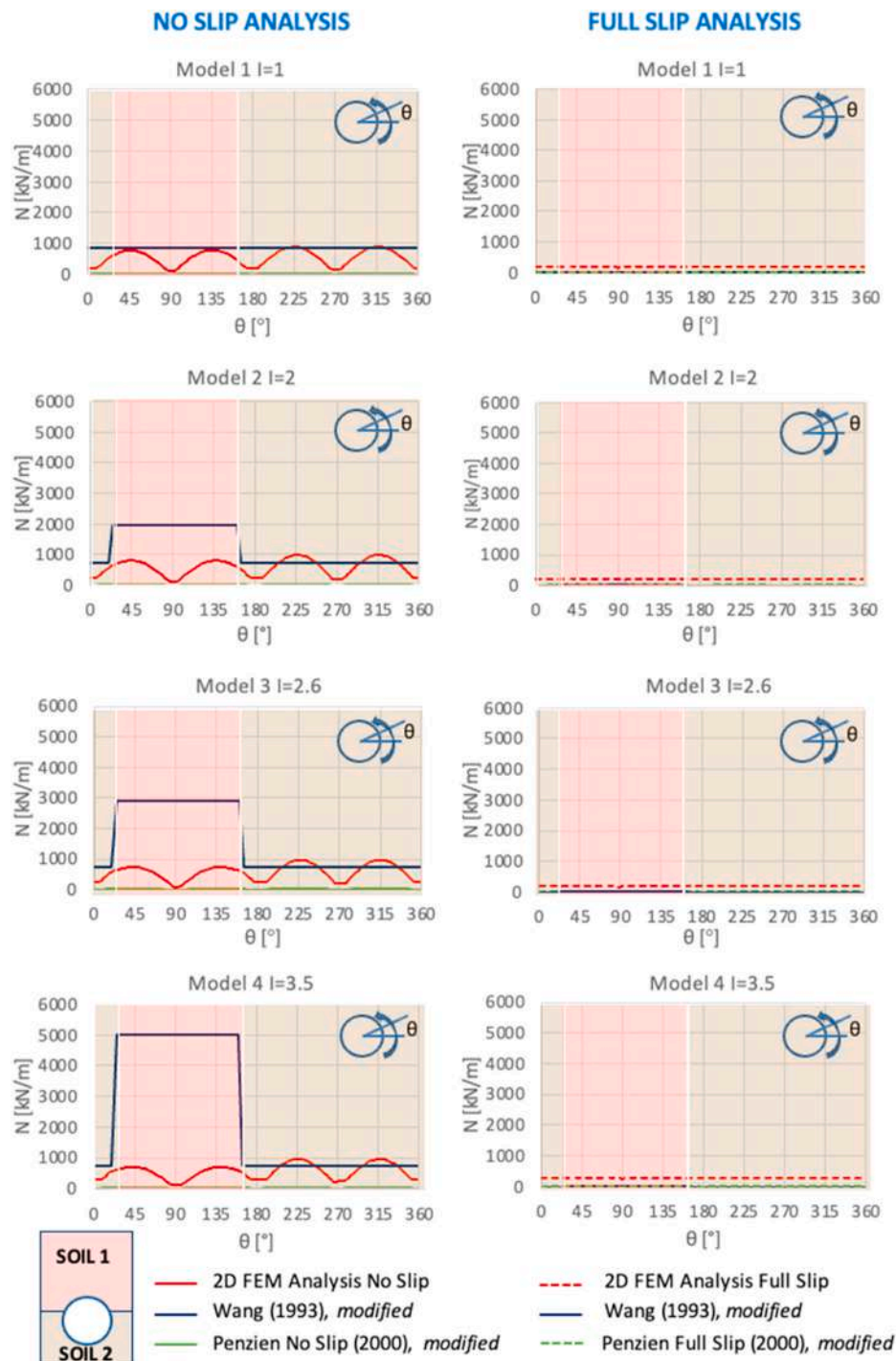
Fig. 10. Comparison between analytical (Approach N.1) and numerical results in terms of dynamic axial forces.

maximum shear strain of the soil at the tunnel depth to be estimated. This strain is evaluated referring to the average value of the maxima soil shear strains that occurred at the tunnel depth. But obviously, a strong soil stiffness discontinuity causes a great difference in the maximum shear strain profile $\gamma_{max}(z)$.

As an example, Fig. 11 a shows the maxima shear strains profile for Model 3 (which refers to the real soil profile), obtained through the FEM analyses. Fig. 11 b shows the zoomed profile for 5 m < z < 35 m. The dashed blue line represents the average value (0.117%) considering both "Soil 1" and "Soil 2". As already specified, this value was used to compute the analytical dynamic lining internal forces shown in Figs. 9 and 10 (see Approach N. 1 in Section 4). The dashed green line represents the average value of the maxima shear strains for every single layer (0.054% for "Soil 1" and 0.165% for "Soil 2", respectively). A great disagreement exists between the dashed blue line and the dashed green line.

So, the analytical internal forces were recalculated using the average values of the maxima shear strains for every single layer, i.e., according to the $\gamma_{max}(z)$ profile represented by the dashed green line of Fig. 11 (see Approach N. 2 in Section 4). Fig. 12 shows the analytical ones evaluated according to Approach N. 2, only for the no-slip condition for Model 3.

The numerical internal forces were also reported. A better agreement between analytical and numerical internal forces was clearly achieved. Similar results were obtained for all the other FEM models (see Section 5.2). The highest degree of difference between $M_{NUM-MAX}$ and the $M_{ANAL-MAX}$ is now equal to about 20% (I = 3.5, Model 4).

Summarizing the analyses concerning Models 1–4 leads to the following conclusions.

- For high values of I, a strongly non-uniform M distribution along the tunnel and important peaks (increasing with the increase in I) at the soil discontinuity were obtained.
- Unlike the bending moments, the axial forces obtained did not vary much with I.
- As regards the three different tunnel-soil interface conditions, very similar results were obtained for each in terms of M, higher values of N were reached in the no-slip condition.
- As for the comparisons between the numerical analyses and the [26, 27] analytical solutions modified by the authors, the best agreement was achieved by means of Approach N. 2, especially in terms of bending moments (ΔM = 0–20%).

5.2. Effects of I on M_{MAX} and N_{MAX}: results concerning models 1–10 (I = 0.3–4.0)

As for Section 5.1, the results reported in this section were obtained considering the 1693 seismic input. Fig. 13 shows the comparison between the maxima analytical internal forces and the numerical ones for all ten models developed (Models 1–10, represented by the numerical

indicators in Fig. 13). Only the no-slip soil-tunnel interface condition was considered. The previously discussed numerical results suggested the use of the no-slip tunnel-soil interface condition to guarantee the highest possible safety condition. Analytical results were obtained using both Approach N. 1 (first row) and Approach N. 2 (second row).

Regarding the bending moments, a good agreement between numerical and analytical results was achieved only for values of I close to 1. The comparison became less satisfactory for strong heterogeneity, see the results for Model 4 (I = 3.5), Model 7 (I = 3.0), Model 9 (I = 0.3) and Model 10 (I = 4.0). This is more evident for the results obtained using Approach N. 1. The highest degree of difference between $M_{NUM-MAX}$ and the $M_{ANAL-MAX}$ is for Model 9 (I = 0.3): it is equal to about 200% using Approach N. 1 and equal to about 20% using Approach N. 2.

As for the dynamic axial forces, the modified Wang solution furnished high values in comparison with the numerical ones for Models 3, 7, 4 and 10. Generally, a better agreement is reached using Approach N. 2. $N_{ANAL-MAX}$ values obtained by the Penzien solution [27] modified according to Approach N. 2 are still too low.

Finally, Fig. 14 reports M_{MAX} and N_{MAX} versus I, adopting both Approach N. 1 and N. 2 and the percentage difference ΔM% between $M_{NUM-MAX}$ and the $M_{ANAL-MAX}$, as well as the percentage difference ΔN% between $N_{NUM-MAX}$ and the $N_{ANAL-MAX}$. Considering that the Penzien solution [27] gives very low values, ΔN% was not considered for the [27].

As for the M_{MAX} vs I trend, it is possible to observe that M_{MAX} strongly depended on I: the further I was away from 1, the higher the value of M_{MAX}, except for Models 5 and 6. The latter furnished values of M_{MAX} lower than those obtained for Model 1 (I = 1.0), because Models 5 and 6 are characterized by a stiffer soil profile along the tunnel in comparison to Model 1 and by a low soil stiffness discontinuity (I = 1.5); then, lower soil shear strains occur around the tunnel for Models 5 and 6 in comparison to those for Model 1. ΔM% is always close to 0 for Model 1 (homogeneous soil crossed by the tunnel), as we expected. Adopting Approach N. 1 for the other models, it ranges between 30% and 60%, except for Model 9 (I = 0.3) for which ΔM% reaches a very high and anomalous value. Adopting Approach N. 2 ΔM% varies in the range 0–20%, except for Model 9, for which ΔM% = 60%. For Model 9 the very soft "Soil 1" produces great localised shear strains in the soil, which in turn produces a great $M_{NUM-MAX}$; this aspect is not completely captured by the analytical Approach N. 2.

As for N_{MAX} vs I trends, it is possible to observe that the numerical axial forces did not significantly vary with I; instead, they strongly increased with I according to the modified Wang solution. Finally, the modified Penzien solution gave very low values, as previously observed. ΔN% is always close to 0 for Model 1. Adopting Approach N. 1, for the other models ΔN% ranges between −10% and −80% and it is farther and farther from zero, the more marked is the difference in stiffness between the two soil layers. Adopting Approach N. 2, ΔN% is remarkably closer to zero for Models 2, 5, 6 and 9, while for the other models it is still quite
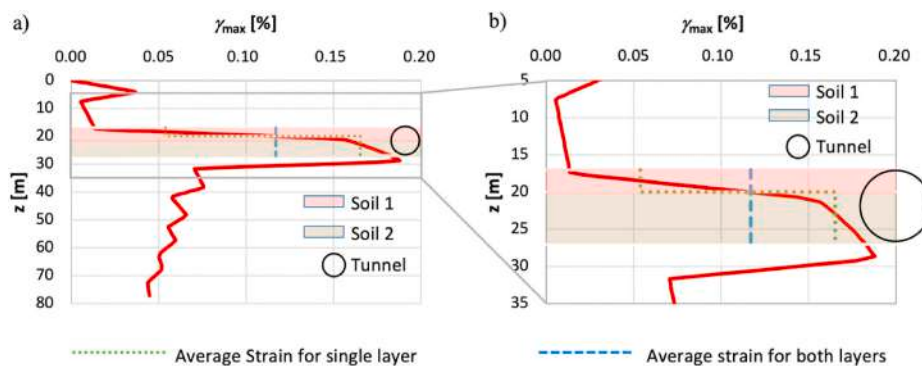

Fig. 11. (a) FEM maxima soil shear strains profile for Model 3 (continuous red line) and soil shear strains adopted for Approach N. 1 (dashed blue line) and for Approach N.2 (dashed green line); (b) Zoomed Profile.
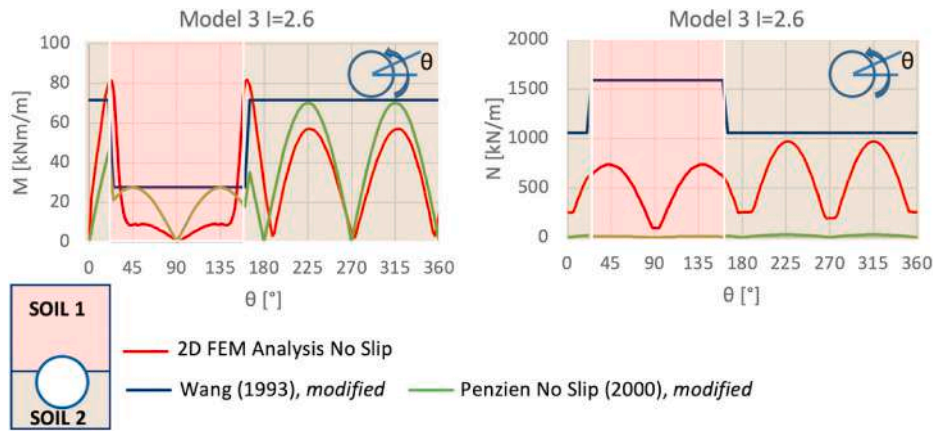
Fig. 12. Comparison between analytical (Approach N. 2) and numerical internal forces for Model 3.
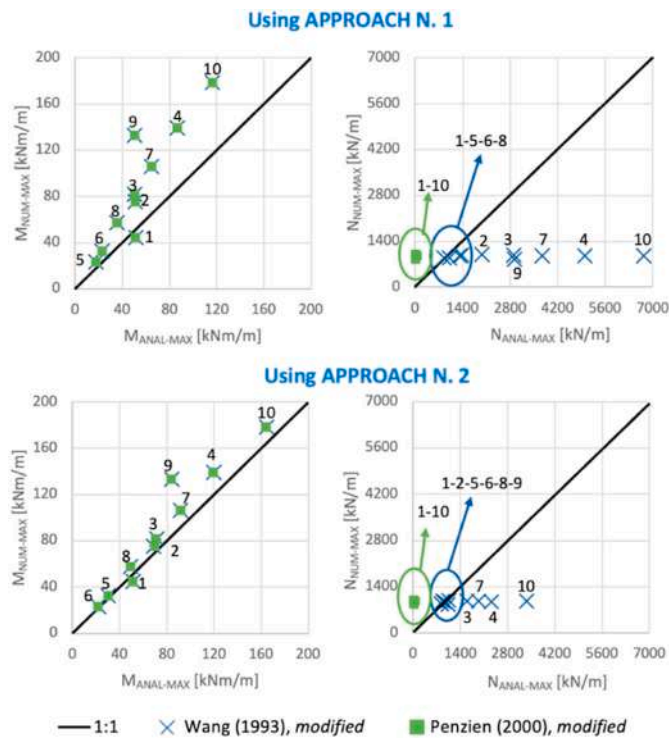

Fig. 13. Maxima numerical and analytical dynamic internal forces. Analytical dynamic internal forces were evaluated considering both Approaches N.1 and N. 2.

far from zero.

Summarizing, the analyses concerning Models 1–10 leads to the following conclusions, confirming generally what was found analysing the previous models.

- A good agreement between numerical and analytical results was achieved using Approach N. 2.
- An increase in I led to an increase in the gap between the analytical and numerical results. The gap could be acceptable in terms of M, but it would not be acceptable in terms of N for a high value of I.
- M_{MAX} strongly depended on I: the further I was away from 1, the higher the value of M_{MAX}. The numerical N_{MAX} did not significantly vary with I; instead, as for the analytical values, N_{MAX} strongly increased with I according to the [26] analytical solution modified by the Authors and assumed very low values according to the [27] analytical solution modified by the authors.

5.3. Effects of the tunnel cover Δz and of the input motion on M and N: results concerning model 3 (I = 2.6)

The effect of the tunnel depth and of the input motion on the dynamic lining forces for tunnels in homogeneous soil were widely investigated by the authors in a previous paper [38]. In the present paper, the authors would like to focus their attention on the effects of the tunnel depth and of the input motion on the dynamic lining forces for tunnels in heterogeneous soil. Including soil heterogeneity, the different values of the tunnel portion interested by Soil 1 and 2 enlighten the effect of the position of the tunnel with respect to the horizontal discontinuity. Varying the tunnel depth, it occurs a double effect since it varies both the tunnel depth and the presence or absence of a soil horizontal discontinuity crossing the tunnel.

The results reported in this section were obtained considering the 1693, 1818 and 1990 seismic inputs, with reference to Model 3 ($\Delta z = 17$ m), Model 3-a ($\Delta z = 12$ m) and Model 3-b ($\Delta z = 7$ m) thus considering the tunnel-soil no-slip condition.

Fig. 15 shows the comparison between the numerical and analytical M_{MAX} (first column) and N_{MAX} (second column), considering the three different tunnel covers: i) $\Delta z = 17$ m (real configuration, Fig. 5); ii) $\Delta z = 12$ m; iii) $\Delta z = 7$ m. So, it was possible to investigate the effect of the tunnel position in respect to the soil stiffness discontinuity. The analytical values were obtained using Approach N.2.

Each histogram shows the influence of the tunnel depth on the dynamic lining forces. For $\Delta z = 7$ m, the tunnel was completely inside "Soil 1", which is a very stiff layer; so, very small shear strains occurred, that in turn produced the lowest values of M_{MAX}. For $\Delta z = 17$ m the highest values of M_{MAX} were obtained, because the tunnel crossed 3 m of "Soil 1" and 7 m of "Soil 2". "Soil 2" is more deformable than "Soil 1" and so "Soil 2" caused the highest shear strains in the tunnel. For $\Delta z = 12$ m the tunnel crossed 8 m of "Soil 1" and 2 m of "Soil 2", so, the soil discontinuity caused bending moments greater than those for $\Delta z = 7$ m, but lower than those for $\Delta z = 17$ m, because for $\Delta z = 12$ m the tunnel crossed only 2 m of "Soil 2" (more deformable of "Soil 1"). Similar results concerned the axial forces N_{MAX}.

These results highlight the importance of evaluating the exact soil profile.

As for the effect of the input motions, which differ only as regards the frequency content (see Section 2.1), it is possible to observe that generally the highest values of M_{MAX} were obtained for the 1818 seismic input. Quite similar values of M_{MAX} were obtained using the 1693 and 1990 seismic inputs. This depends on the soil-nonlinearity discussed in Section 3.

The input motions differ for the frequency content and thus they cause in the soil different strain levels, which in turn lead to different operative G_s and D_s values due to soil nonlinearity. The different
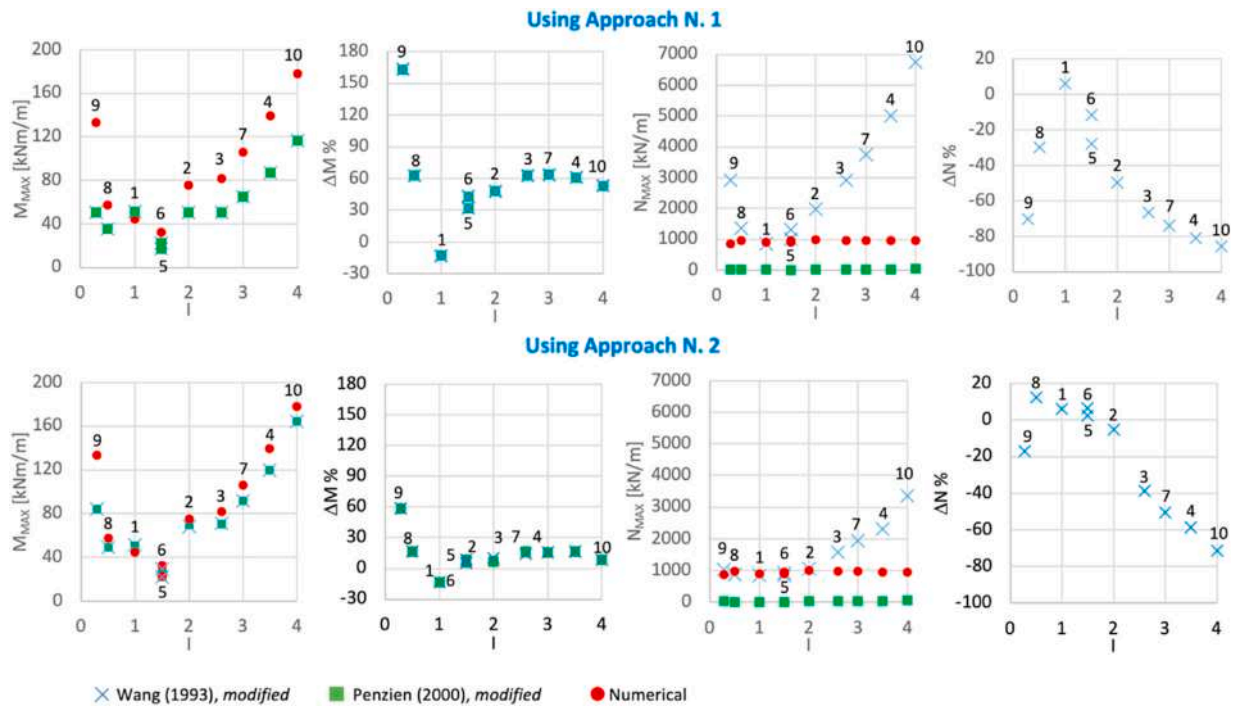
Fig. 14. Maxima numerical and analytical internal forces versus soil impedance ratio and their percentage differences.

operative G_s and D_s values lead to different soil natural frequencies. The closer the predominant frequency of the input is to the natural frequency of the soil, the higher the strains will be. Thus, a circular process occurs, until a final configuration is reached. This circular process is different for the three input motions. Operative G_s and D_s reported in Table 5 were used to consider the soil nonlinearity. As previously discussed, these values depend on the soil strain levels that in turn depend on the seismic inputs (see Fourier Spectra in Fig. 4).

From Table 5 it is possible to observe that: $G_{s1}/G_{s2} = 5.24$ for the 1693 seismic input, $G_{s1}/G_{s2} = 6.05$ for the 1818 seismic input, and $G_{s1}/G_{s2} = 5.18$ for the 1990 seismic input. So, the highest impedance ratio I was obtained considering the 1818 seismic input. This in turn causes the highest values of M_{MAX}. Similar trend was observed in terms of N_{MAX} except for the modified Wang approach at 17 m tunnel depth where 1693 seismic input has the highest N_{MAX}.

So, the results reported in Fig. 15 underline the importance of carefully considering soil nonlinearity. Soil nonlinearity has been considered approximately in the present paper, due to a lack of all the geotechnical data necessary for using more sophisticated soil constitutive models including dynamic soil nonlinearity [90,91] and because the main goal of the paper is to evaluate the effects of soil heterogeneity (i. e., of the I value) at the tunnel level in the dynamic tunnel lining forces.

6. Conclusions

Starting from a real case history regarding a cross-section of the Catania (Italy) underground network crossing two different soil layers ("Soil 1" and "Soil 2"), the paper deals with several numerical FEM analyses, focusing attention on the soil discontinuity at the tunnel depth, in terms of the soil impedance ratio I, evaluated as the ratio between the impedance $\rho_1 \bullet V_{s1}$ of the soil interacting with the upper part of the tunnel ("Soil 1") and the impedance $\rho_2 \bullet V_{s2}$ of the soil interacting with the bottom part of the tunnel ("Soil 2"), being ρ and V_S the soil density and shear waves velocity, respectively. Different values of the impedance ratio I and of the tunnel cover Δz were assumed. The tunnel dynamic lining bending moment (M) and axial force (N) were investigated.

Moreover, the analytical solutions proposed by Refs. [26,27] to compute M and N for tunnels in homogeneous soil deposits were

considered and modified to include soil heterogeneity. Two different approaches were proposed to evaluate the maxima shear strain (γ_{max}) required by the analytical solutions: i) an average value of γ_{max} along the tunnel was used in Approach N. 1; ii) the average value of γ_{max} for "Soil 1" along the upper part of the tunnel and the average value of γ_{max} for "Soil 2" along the lower part of the tunnel were used in Approach N. 2. The results obtained by both Approaches N.1 and N.2 were compared with the FEM results.

The main results can be summarised as follows.

- The strong influence of the heterogeneity of the soil crossed by the tunnel was found in the M distribution. The further I was away from 1, the higher the value of M_{MAX}, obtaining a strongly non-uniform M distribution along the tunnel.
- Unlike the bending moments, the axial forces obtained did not vary significantly with I.
- As for the comparisons with the [26,27] analytical solutions modified by the authors, a good agreement was achieved for values of I close to 1 and using Approach N. 2.
- In the case of strong soil impedance discontinuity at the tunnel depth (I very far from 1), it is advisable not to use either the original [26, 27] solutions or those modified according to the proposed Approach N.1; it is advisable to use the solutions [26,27] modified according to the proposed Approach N. 2 for a preliminary estimation of the dynamic lining forces M. For a careful estimation of the dynamic lining forces M and N it is advisable to perform FEM analyses.
- As for the effect of the tunnel position with respect to the soil impedance discontinuity on M and N, the lowest values of M_{MAX} were obtained for the tunnel completely inside "Soil 1", which is a very stiff layer. The highest values of M_{MAX} were obtained when the tunnel crosses a greater portion of the more deformable "Soil 2" than the stiffer "Soil 1". Similar results concerned the axial forces N_{MAX}, even if the tunnel depth proved to have a minor influence.
- The results obtained highlight the importance of evaluating the exact soil profile and the soil impedance ratio I around tunnels through careful geotechnical investigations.
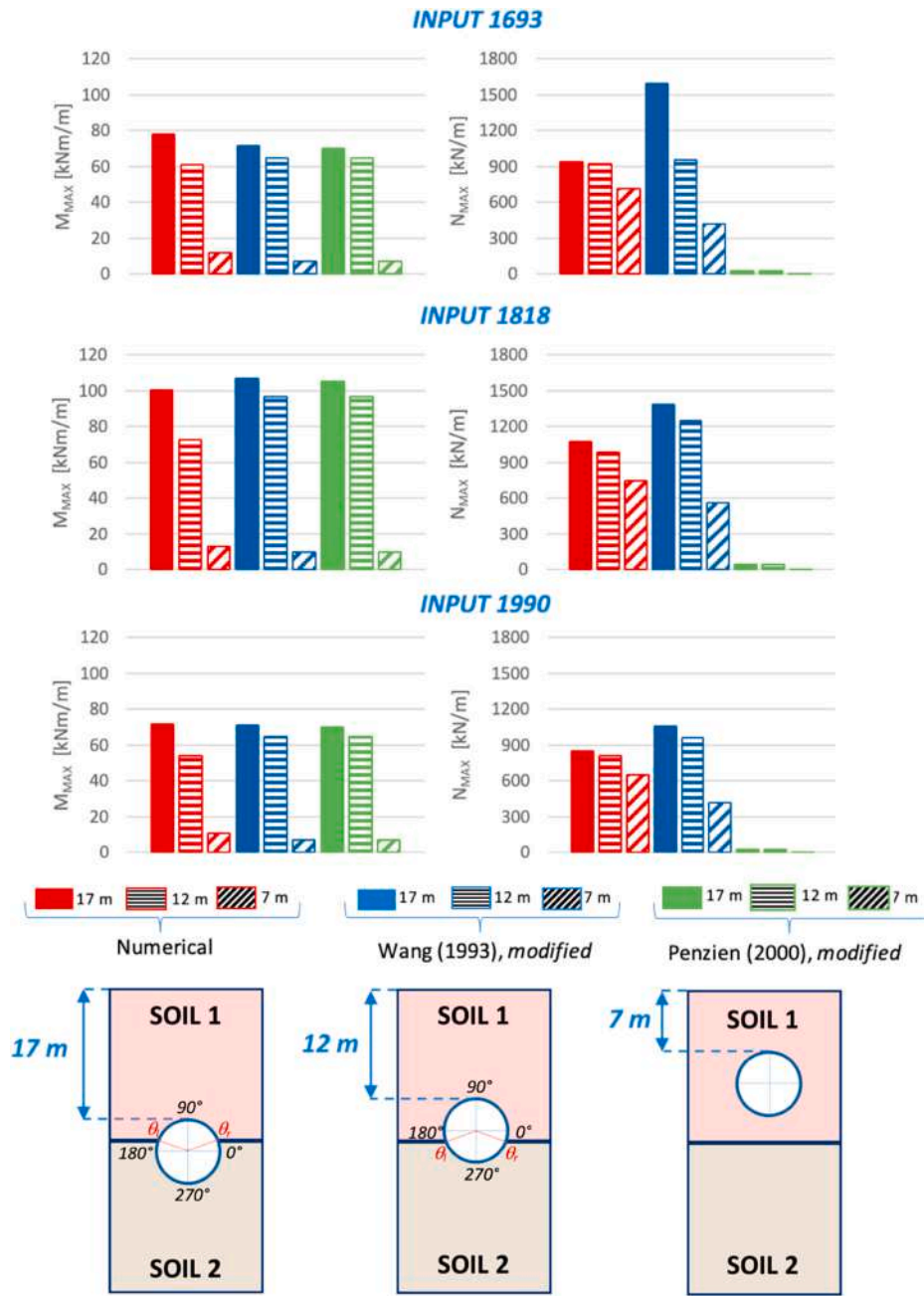
Fig. 15. Maxima numerical and analytical internal forces for different tunnel depths and input motions.

Author statement

The authors confirm contribution to the paper as follows: study conception and design: G. Abate, S. Grasso, M.R. Massimino; data collection: G. Abate, S. Grasso, M.R. Massimino; Formal analysis and interpretation of results: G. Abate, S. Grasso, M.R. Massimino; draft manuscript preparation: G. Abate, S. Grasso, M.R. Massimino. All authors reviewed the results and approved the final version of the manuscript.

Declaration of competing interest

The authors declare that they have no known competing financial interests or personal relationships that could have appeared to influence the work reported in this paper.

Data availability

The authors are unable or have chosen not to specify which data has been used.

References

[1] Dowding CH, Rozen A. Damage to rock tunnels from earthquake shaking. J Geotech Eng Div, ASCE 1978;104(GT2):175–91.

[2] Power M, Rosidi D, Kaneshiro J, Gilstrap S, Chiou SJ. Summary and evaluation of procedures for the seismic design of tunnels. Final Report for Task 112-d-5.3(c). Buffalo, New York: National Centre for Earthquake Engineering Research; 1998.

[3] Massimino MR, Abate G, Corsico S, Louarn R. Comparison between two approaches for non-linear fem modelling of the seismic behaviour of a coupled soil-structure system. Geotech Geol Eng 2019;37(3):1957–75. https://doi.org/10.1007/s10706-018-0737-y.

[4] Massimino MR, Abate G, Grasso S, Pitilakis D. Some aspects of DSSI in the dynamic response of fully-coupled soil-structure systems. Riv Ital Geotec 2019;1:44–70. https://doi.org/10.19199/2019.1.0557-1405.044. ISSN: 0557-1405.

[5] Andreotti G, Lai CG. Use of fragility curves to assess the seismic vulnerability in the risk analysis of mountain tunnels. Tunn Undergr Space Technol 2019;91. https://doi.org/10.1016/j.tust.2019.103008.

[6] Owen GN, Scholl RE. Earthquake engineering of large underground structures, prepared for the federal highway administration. 1981. FHWA/RD-80/195.

[7] Sharma S, Judd WR. Underground opening damage from earthquakes. Eng Geol 1991;30:263–76.

[8] Hashash YMA, Hook JJ, Schmidt B, Yao JI-C. Seismic design and analysis of underground structures. Tunn Undergr Space Technol 2001;16(2):247–93.

[9] Kontoe S, Zdravkovic L, Potts D, Mentiki C. Case study on seismic tunnel response. Can Geotech J 2008;45:1743–64.

[10] Wang ZZ, Gao B, Jiang YJ, Yuan S. Investigation and assessment on mountain tunnels and geotechnical damage after the Wenchuan earthquake. Sci China Technol Sci 2009;52(2):549–58.

[11] Gazetas G. Case histories of tunnel failures during earthquakes and during construction, proc. Of the half-day conference, A tunnel/underground station failure conference. the Israeli Geotechnical Society; 19 January 2014.

[12] Lu CC, Hwang JH. Damage analysis of the new Sanyi railway tunnel in the 1999 Chi-Chi earthquake: necessity of second lining reinforcement. Tunn Undergr Space Technol 2018;73:48–59.

[13] Lu CC, Hwang JH. Nonlinear collapse simulation of Daikai Subway in the 1995 Kobe earthquake: necessity of dynamic analysis for a shallow tunnel. Tunn Undergr Space Technol 2019;87:78–90.

[14] De Silva F, Fabozzi S, Nikitas N, Bilotta E, Fuentes R. Seismic vulnerability of circular tunnels in sand. Geotechnique 2021;71(11):1056–70.

[15] Kawashima K. In: Fujita Miyazaki, editor. Seismic design of underground structures in soft ground: a review. Geotechnical aspects of underground construction in soft ground. Rotterdam: Balkema; 2000.

[16] Deere DU, Pec RB, Parker HW, Monsees JE, Schmidt B. Design of tunnel support systems, 49th annual meeting of the highway research board. United States: Washington District of Columbia; 1970.

[17] Hudoba I. Contribution to static analysis of load-bearing concrete tunnel lining built by shield-driven technology. Tunn Undergr Space Technol 1997;12(1):55–8.

[18] Vassilis K, Papanikolaoua AJ, Kappos. Practical nonlinear analysis of unreinforced concrete tunnel linings. Tunn Undergr Space Technol 2014;40:127–40.

[19] Do NA, Dias D. Tunnel lining design in multi-layered grounds. Tunn Undergr Space Technol 2018;81:103–11.

[20] ISO 23469. Bases for design of structures - seismic actions for designing geotechnical works. International Organisation for Standardisation; 2005.

[21] AFPS/AFTES. Guidelines on earthquake design and protection of underground structures, Working group of the French association for seismic engineering (AFPS) and French Tunnelling Association (AFTES) Version 1. 2001.

[22] FHWA. Technical manual for design and construction of road tunnels – civil elements. U.S. Department of Transportation, Federal Highway Administration, Publication No. FHWA-NHI-09-010; March 2009.

[23] Amorosi A, Boldini D, Falcone G. Numerical prediction of tunnel performance during centrifuge dynamic tests. Acta Geotech 2014;9(4):581–96. https://doi.org/10.1007/s11440-013-0295-7.

[24] Bilotta E, Lanzano G, Madabhushi SPG, Silvestri F. A numerical Round Robin on tunnels under seismic actions. Acta Geotech 2014;9(4):563–79. https://doi.org/10.1007/s11440-014-0330-3.

[25] Tsinidis G, de Silva F, Anastasopoulos I, Bilotta E, Bobet A, Hashash YMA, He C, Kampas G, Knappett J, Madabhushi G, Viggiani G, Fuentes R. Seismic behaviour of tunnels: from experiments to analysis. Tunn Undergr Space Technol 2020;99. https://doi.org/10.1016/j.tust.2020.103334.

[26] Wang JN. Seismic design of tunnels: a state-of-the-art approach. In: Monograph, monograph 7. Parsons, brinckerhoff. New York: Quade and Douglas Inc; 1993.

[27] Penzien J. Seismically-induced racking of tunnel linings. Earthq Eng Struct Dynam 2000;29:683–91.

[28] Pitilakis K, Tsinidis G, Leanza A, Maugeri M. Seismic behaviour of circular tunnels accounting for above-ground structures interaction effects. Soil Dynam Earthq Eng 2014;67:1–15.

[29] Fabozzi S, Catalano S, Falcone G, Naso G, Pagliaroli A, Peronace E, Porchia A, Romagnoli G, Moscatelli M. Stochastic approach to study the site response in presence of shear wave velocity inversion: application to seismic microzonation studies in Italy. Eng Geol 2020;280:105914. https://doi.org/10.1016/j.enggeo.2020.105914.

[30] Fu J, Liang J, Qin L. Dynamic soil-tunnel interaction in layered half-space for incident P- and SV-waves. Earth Sci 2015;28(4):275–84.

[31] Liang J, Zhu J. A FE-IBE method for linearized nonlinear soil-tunnel interaction in water-saturated, poroelastic half-space: II. A revisit to two widely used analytical solutions. Soil Dynam Earthq Eng 2019;120:468–78.

[32] Zhu J, Liang J, Ba Z. A 2.5D equivalent linear model for longitudinal seismic analysis of tunnels in water-saturated poroelastic half-space. Comput Geotech 2019;109:166–88.

[33] Bathe KJ. Nonlinear finite element analysis and ADINA. In: Proc. of the 12th ADINA Conf. on computers and structures; 1999.

[34] ADINA. Automatic dynamic incremental nonlinear analysis. Theory and modelling guide. USA: ADINA R&D, Inc. Watertown; 2008.

[35] Hashash YMA, Park D, Yao JIC. Ovaling deformations of circular tunnels under seismic loading, an update on seismic design and analysis of underground structures. Tunn Undergr Space Technol 2005;20:435–41.

[36] Abate G, Corsico S, Massimino MR. FEM modelling of the seismic behaviour of a tunnel-soil-aboveground building system: a case history in Catania (Italy). Procedia Eng 2016;158:380–5. https://doi.org/10.1016/j.proeng.2016.08.459. ISSN: 1877-7058.

[37] Abate G, Massimino MR. Numerical modelling of the seismic response of a tunnel–soil–aboveground building system in Catania (Italy). Bull Earthq Eng 2017;15(1):469–91.

[38] Abate G, Massimino MR. Parametric analysis of the seismic response of coupled tunnel–soil–aboveground building systems by numerical modelling. Bull Earthq Eng 2017;15(1):443–67.

[39] Atkinson JH, Potts DM. Subsidence above shallow tunnels in soft ground. J Geotech Eng Div ASCE 1977;GT4:307–25.

[40] Attewell PB. Proc. Conf. On large ground movements and structures. In: Ground movements caused by tunnelling in soil. Cardiff; July 1978. p. 812–948.

[41] Attewell PB, Taylor RK. Ground movements and their effects on structures. 1984. p. 132–212.

[42] Anagnostou G, Kovari K. The face stability of slurry-shield driven tunnels. Tunn Undergr Space Technol 1994;9(2):165–74.

[43] Burland JP. Assessment of risk of damage to buildings due to tunnelling and excavation. In: Proc. First Int. Conf. on Earthquake Geotechnical Engineering of Tokyo November 1-12. Earthquake Geotechnical Engineering; 1995. p. 1189–202.

[44] Broere W. Influence of excess pore pressures on the stability of the tunnel face. Geotechnical Aspects of Underground Construction in Soft Ground 2002:179–84. Toulouse, France.

[45] Mohammadi J. Tunnel face stability analysis in soft ground by EPB method (case study: tehran metro line 7). Tehran, Iran: M'Sc Thesis; 2010.

[46] Carranza-Torres C, Reich T, Saftner D. Proc. 61st Minnesota annual geotechnical engineering conference. In: Stability of shallow circular tunnels in soils using analytical and numerical models. St. Paul Campus: University of Minnesota; February 22, 2013.

[47] Abate G, Corsico S, Grasso S, Massimino MR, Pulejo A. Analysis of the vibration induced by a TBM to refine soil profile during tunnelling: the Catania case history. Tunnels and Underground Cities: engineering and Innovation meet Archeology, Architecture and Art. Proc. of the WTC 2019 ITA-AITES World Tunnel Congress 2019:567–76.

[48] Abate G, Grasso S, Massimino MR. The role of shear wave velocity and non-linearity of soil in the seismic response of a coupled tunnel-soil-above ground building system. Geosciences 2019;9(11):1–25. 473.

[49] Abate G, Corsico S, Grasso S, Massimino MR. An early-warning system to validate the soil profile during TBM tunnelling. Geosciences 2022;12(113):1–21. https://doi.org/10.3390/geosciences12030113.

[50] Caruso M, Ferraro A, Grasso S, Massimino MR. Site response analysis in eastern Sicily based on direct and indirect vs measurements. In: Daponte P, Simonelli AL, Code, editors. Proc. 1st IMEKO TC4 int. Workshop on metrology for geotechnics, MetroGeotechnics, vol. 121564. Benevento; Italy; 2016, ISBN 978-929900750-1. p. 115–24. 17-18 March 2016.

[51] Castelli F, Grasso S, Lentini V, Massimino MR. Proc. 1st IMEKO TC4 int. Workshop on metrology for geotechnics. In: In situ measurements for evaluating liquefaction potential under cyclic loading. Metro Geotechnics; 2016. p. 79–84.

[52] Castelli F, Cavallaro A, Ferraro A, Grasso S, Lentini V, Massimino MR. Static and dynamic properties of soils in Catania (Italy). Ann Geophys 2018;61(2):SE221.

[53] Cavallaro A, Grasso S, Maugeri M. Volcanic soil characterization and site response analysis in the city of Catania. Proc. 8th Nat. Conf. on Earthquake Engineering 18–22 April 2006:835–44. San Francisco, California, USA.

[54] Cavallaro A, Ferraro A, Grasso S, Maugeri M, Santini A, Moraci N. Site response analysis of the Monte Po hill in the city of Catania. AIP Conf Proc 2008;1020: 240–51.

[55] Cavallaro A, Ferraro A, Grasso S, Maugeri M. Topographic effects of the Monte Po hill in Catania. Soil Dynam Earthq Eng 2012;43:97–113.

[56] Ferraro A, Grasso S, Massimino MR. Site effects evaluation in Catania (Italy) by means of 1-D numerical analysis. Ann Geophys 2018;61(2):SE224. https://doi.org/10.4401/ag-7708.

[57] Faccioli E, Pessina V. In: Faccioli E, Pessina V, editors. The Catania Project: earthquake damage scenarios for a risk area in the Mediterranean. CNR - gruppo Nazionale per la Difesa dei Terremoti, ISBN 88-900449-0-X.

[58] NTC 2018: D.M. 17/01/18 - updating of technical standards for buildings. 17th January Off J Italian 2018 [in Italian].

[59] ENV EC8 2003: design of structures for earthquake resistance. European Pre-standard; 1998 [Europ. Com. for Standard. Bruxelles].

[60] Maugeri M. Advances in earthquake engineering. In: Seismic prevention of damage: a case study in a Mediterranean city. Southampton, UK: WIT Press; 2005. Volume 14, Boston, Mass.

[61] Grasso S, Maugeri M. Vulnerability of physical environment of the city of Catania using GIS technique. In: Maugeri M, editor. Seismic prevention of damage: a case study in a mediterranean city. Southampton, UK: WIT Press; 2005. p. 155–75. Chapter IX.

[62] Grasso S, Laurenzano G, Maugeri M, Priolo E. Seismic response in Catania by different methodologies. In: Maugeri M, editor. Seismic prevention of damage: a case study in a mediterranean city. Southampton, UK: WIT Press; 2005. p. 63–79. Chapter IV.

[63] Cavallaro A, Grasso S, Ferraro A. A geotechnical engineering study for the safeguard, restoration and strengthening of historical heritage. Procedia Eng 2016; 158:134–9.

[64] Massimino MR, Abate G, Corsico S, Grasso S, Motta E. Dynamic behaviour of coupled soil-structure systems by means of fem analysis for the seismic risk mitigation of INGV building in Catania (Italy). Special Issue, Ann Geophy 2018;61: 21–5. 2018.

[65] Grasso S, Massimino MR. A GIS for data mining in seismic microzonation studies. Smart Innov. Syst. Technol. 2019;142:191–201.

[66] Seed HB, Idriss IM. Report EERC 70-10, earthquake engineering research center. In: Soil moduli and damping factors for dynamic response analyses. Berkeley: University of California; 1970.

[67] Vucetic M, Dobry R. Effect of soil plasticity on cyclic response. J Geotech Eng 1991; 117(1):89–107.

[68] Darendeli MB. Geotechnical engineering report GD01-1. In: Development of a new family of normalized modulus reduction and material damping curves. Austin, TX, USA: University of Texas at Austin; 2001.

[69] Azzaro R, Barbano MS, Moroni A, Mucciarelli M, Stucchi M. The seismic history of Catania. J Seismol 1999;3(3):235–52.

[70] Azzaro R, Barbano MS. Seismogenetic features of SE sicily and scenario earthquakes for Catania. The Catania project: earthquake damage scenarios for a high-risk area in the mediterranean, part I: seismotectonic framework and earthquake scenarios. Roma: CNR-Gruppo Nazionale per la Difesa dai Terremoti; 2000. p. 9–13.

[71] Grassi F, Massimino MR. Evaluation of kinematic bending moments in a pile foundation using the finite element approach. WIT Trans Built Environ 2009;104: 479–88.

[72] Kirtas E, Rovithis E, Pitilakis K. Subsoil interventions effect on structural seismic response. Part I: validation of numerical simulations. J Earthq Eng 2009;13: 155–69.

[73] Maugeri M, Abate G, Massimino MR. Soil-Structure interaction for seismic improvement of noto cathedral (Italy). Geotech Geol Earthq 2012;16:217–39.

[74] Abate G, Massimino MR, Maugeri M. Numerical Modelling of centrifuge tests on tunnel-soil systems. Bull Earthq Eng 2015;13(7):1927–51.

[75] Fiamingo A, Bosco M, Massimino MR. The role of soil in structure response of a building damaged by the 26 December 2018 earthquake in Italy. J Rock Mech Geotech Eng 2022. https://doi.org/10.1016/j.jrmge.2022.06.010. ISSN 1674-7755.

[76] Lanzo G, Silvestri F. Risposta sismica locale: teorie ed esperienze. Napoli: Helvius Edizioni; 1999.

[77] Zienkiewicz OC, Bicanic N, Shen FQ. Adv comput nonlinear mech. In: Earthquake input definition and the transmitting boundary conditions. Vienna: Springer Vienna; 1989. p. 109–38.

[78] Gajo A, Muir Wood D. Report of ECOEST project. In: Numerical analysis of behaviour of shear stacks under dynamic loading. EERC laboratory, Bristol University; 1997.

[79] Amorosi A, Boldini D, di Lernia A. Dynamic soil-structure interaction: a three-dimensional numerical approach and its application to the Lotung case study. Comput Geotech 2017;90:34–54. https://doi.org/10.1016/j.compgeo.2017.05.016.

[80] Lysmer J, Kuhlemeyer RL. Finite dynamic model for infinite media. J Eng Mech Div ASCE 1969;95(4):859–78.

[81] Sedarat H, Kozak A, Hashash YMA, Shamsabadi A, Krimotat A. Contact interface in seismic analysis of circular tunnels. Tunn Undergr Space Technol 2009;24(4): 482–90.

[82] Pitilakis K, Tsinidis G. Performance and seismic design of underground structures. In: Maugeri M, Soccodato C, editors. Earthquake geotechnical engineering design. Geotechnical, vol. 28. Geological and Earthquake Engineering; 2014. p. 279–340.

[83] Esmaeilzadeh Seylabi E, Jeong C, Taciroglu E. On numerical computation of impedance functions for rigid soil-structure interfaces embedded in heterogeneous half-spaces. Comput Geotech 2016;72:15–27.

[84] Nguyen KT, Kusanovic DS, Asimaki D. Dynamic soil impedance functions for cylindrical structures buried in elastic half-space. Soil Dynam Earthq Eng 2022; 162:107431.

[85] Chopra AK. Dynamics of structures, theory and applications to earthquake engineering. Beijing: Higher Education Press; 2007.

[86] Hashash YMA, Park D. Viscous damping formulation and high-frequency motion propagation in non-linear site response analysis. Soil Dynam Earthq Eng 2002;22 (7):611–24.

[87] Amorosi A, Boldini D, Elia G. Parametric study on seismic ground response by finite element modelling. Comput Geotech 2010;37(4):515–28. https://doi.org/ 10.1016/j.compgeo.2010.02.005.

[88] Argyroudis S, Tsinidis G, Gatti F, Pitilakis K. Effects of SSI and lining corrosion on the seismic vulnerability of shallow circular tunnels. Soil Dynam Earthq Eng 2017; 98:244–56. https://doi.org/10.1016/j.soildyn.2017.04.016.

[89] Merritt JL, Monsees JE, Hendron AJ Jr. Seismic design of underground structures, Proc. of the 1985 Rapid Excavation Tunnelling Conference, 1, 104 -131..

[90] Abate G, Caruso C, Massimino MR, Maugeri M. Validation of a new soil constitutive model for cyclic loading by fem analysis. Solid Mech Appl 2007;146:759–68.

[91] Abate G, Massimino MR, Maugeri M, Muir Wood D. Numerical modelling of a shaking table test for soil-foundation-superstructure interaction by means of a soil constitutive model implemented in a FEM code. Geotech Geol Eng 2010;28(1): 37–59.